γ-ray production by proton and α-particle induced reactions on ^{12}C, ^{16}O, ^{24}Mg, and Fe

A. Belhout
USTHB, Faculté de Physique, BP 32, El-Alia, 16111 Bab Ezzouar, Algiers, Algeria

J. Kiener,[*] A. Coc, J. Duprat, C. Engrand, C. Fitoussi,[†] M. Gounelle,[‡] A. Lefebvre-Schuhl, N. de Séréville,[§] V. Tatischeff, and J.-P. Thibaud
Centre de Spectrométrie Nucléaire et de Spectrométrie de Masse (CSNSM), CNRS-IN2P3 et Université Paris-Sud, F-91405 Orsay Campus, France

M. Chabot and F. Hammache
Institut de Physique Nucléaire (IPN), CNRS-IN2P3 et Université Paris-Sud, F-91400 Orsay, France

H. Benhabiles-Mezhoud[‖]
Département de Physique, Université de Boumerdes, Avenue de l'Indépendance, 35000 Boumerdes, Algeria
(Received 30 March 2007; published 20 September 2007)

γ-ray production cross sections for proton and α-particle interactions with ^{12}C, ^{16}O, ^{24}Mg, and Fe have been measured in the energy range 5–25 MeV with proton beams and 5–40 MeV with α-particle beams. Isotopically pure foils of ^{24}Mg and foils of natural isotopical composition of C, MgO, and Fe have been used. γ-ray angular distributions were obtained with five high-purity Ge detectors with bismuth germanate Compton shields placed at angles of 45° to 157.5°. Cross sections for more than 50 different γ-ray transitions were extracted, and for many of them no data have been published before. Comparison of present data with data available in the literature shows mostly good to excellent agreement. In addition to the production cross sections, high-statistics, low-background line shapes of the 4.438 MeV ^{12}C γ ray from inelastic scattering off ^{12}C and spallation of ^{16}O were obtained. Comparison with nuclear reaction calculations shows that these data place interesting constraints on nuclear reaction models.

DOI: 10.1103/PhysRevC.76.034607 PACS number(s): 23.20.En, 24.10.−i, 25.10.+s, 96.60.qe

I. INTRODUCTION

Nuclear γ-ray lines produced by accelerated ions in solar flares carry important information on the energetic particle properties and the isotopic composition of the interaction region at the solar surface. The intensities of the different narrow interaction lines, principally produced by interactions of accelerated protons and α particles, depend on the relative abundances of ambient nuclei, the abundance ratio of the two light particles, and their energy spectrum [1]. Another signature of the energetic particle composition can be found in the line profiles. The shapes of the nuclear interaction lines reflect the recoil momentum distributions of the γ-ray emitting nuclei. From these the mass and directional distribution of the interacting energetic particles can be inferred with the aid of detailed nuclear reaction calculations [2].

Several satellites equipped with scintillation detectors reported a wealth of solar flare γ-ray spectra mainly during the period 1980 to 2000. Prominent nuclear deexcitation lines from the abundant nuclei ^{12}C, ^{16}O, ^{20}Ne, ^{24}Mg, ^{28}Si, and ^{56}Fe, the ^{7}Li-^{7}Be line feature around 450 keV from $\alpha + \alpha$ interactions, as well as the neutron-capture line on hydrogen and the positron annihilation line could be observed in many flares [3]. Besides interesting abundance determinations of the emitting nuclei [4,5], the position and width of some strong nuclear lines revealed interesting constraints on the directional distribution of the accelerated particles [6,7]. The full potential of line-shape analysis, however, was not possible with these data taken by scintillation detectors, which have only modest energy resolution.

In 2002, two satellites dedicated to γ-ray astronomy were successfully launched. The Reuven Ramaty high-energy solar spectroscopic imager (RHESSI) [8] investigates high-energy phenomena on the sun, and the International γ-Ray Astrophysics Laboratory (INTEGRAL) [9] observes x- and γ-ray emissions from galactic and extragalactic sources. Both are equipped with γ-ray telescopes based on high-resolution germanium detectors. This opened up for the first time the possibility of obtaining resolved line profiles from, e.g., accelerated proton and α-particle interactions in solar flares.

The period of strong solar activity in October-November 2003 produced some of the most intense X-class solar flares with γ-ray emission obtained so far. RHESSI and INTEGRAL, although the latter instrument was not designed for solar flare

[*]Jurgen.Kiener@csnsm.in2p3.fr
[†]Present address: Institute of Isotope Geochemistry and Mineral Resources, Departement of Earth Sciences, ETH Zürich, Haldenbachstrasse 44, 8092 Zürich, Switzerland.
[‡]Present address: Laboratoire d'Etude de la Matière Extraterrestre, Muséum National d'Histoire Naturelle, 57 rue Cuvier, F-75005 Paris.
[§]Present address: Institut de Physique Nucléaire (IPN), CNRS-IN2P3 et Université Paris-Sud, F-91400 Orsay, France.
[‖]Present address: Centre de Spectrométrie Nucléaire et de Spectrométrie de Masse (CSNSM), CNRS-IN2P3 et Université Paris-Sud, F-91405 Orsay, France.

investigations, obtained spectra from several flares of this period. In particular, the spectrum of the October 28, 2003, solar flare observed by INTEGRAL/SPI shows prominent nuclear lines at 2.2, 4.4, and 6.1 MeV with good statistics [10]. Analysis of the line profiles and their interpretation in terms of the energetic particle properties need reliable predictions of the line profiles resulting from nuclear reactions. This may be achieved by systematically comparing the measured line profiles against the line profiles resulting from nuclear reaction calculations, adjusting thereby a set of parameters describing the optical potential for the direct reaction mechanism and the contribution of compound nucleus resonances as a function of projectile energy.

We concentrated on the 4.438 MeV line of ^{12}C, mainly produced in solar flares by proton and α-particle induced reactions on ^{12}C and ^{16}O. For proton reactions with these nuclei, lines shapes were available in much of the interesting energy range [11–13], while no line shapes were available for α-particle reactions. We therefore completed the database by measuring line shapes produced by α particles incident on ^{12}C and ^{16}O from threshold to 37.5 MeV and for some proton energies not covered in previous experiments.

Another important feature of the energetic particle spectrum is its heavy-ion content. Accelerated heavy ions interacting with the hydrogen and helium of the solar atmosphere produce in inverse kinematics the same nuclear deexcitation lines as the energetic protons and α particles. The lines are, however, strongly broadened because of the much higher velocities of the emitting nuclei and therefore cannot easily be extracted from solar flare spectra. Subtracting the prominent narrow lines and a continuum component from electron bremsstrahlung, Share and Murphy [14] obtained a spectrum composed of such broad lines from accelerated heavy ions and a component from unresolved weak lines.

These weak lines are produced—like the prominent narrow lines—by proton and α-particle reactions with ambient nuclei; but unlike the resolved strong lines, which are from the deexcitation of the first few excited levels in nuclei, these unresolved lines are from the numerous possible transitions from higher lying levels. These lines also have low cross sections and form a quasicontinuum component in solar flare spectra. The shape of this component, however, is very uncertain because of the scarcity of experimental data, which complicates considerably the determination of the broad-line fluxes.

The most important target nuclei for this component are the abundant isotopes for which the reaction products have reasonably high density of γ-ray-emitting excited levels. These nuclei are in particular ^{20}Ne, ^{24}Mg, ^{28}Si, and ^{56}Fe. Among these nuclei, we measured the γ-ray production for proton and α-particle induced reactions with ^{24}Mg and Fe at several energies to investigate the role of the different reaction mechanisms contributing to the population of the high-lying excited levels in the reaction products.

The experiment and the data analysis are described in Secs. II and III, respectively. Measured line profiles and cross sections are presented in Sec. IV and compared with nuclear reaction calculations in Sec. V. A summary is provided in Sec. VI.

II. EXPERIMENT

The experiment was done at the 14-MV tandem Van-de-Graaff accelerator of the Institut de Physique Nucléaire Orsay. Proton and α-particle beams were directed onto self-supporting target foils of C, ^{24}Mg, and Fe and of MgO mounted on a thin Al foil, and onto a small piece of the Allende meteorite. The different targets were fixed onto brass frames and arranged on a multiple target holder, which could be shifted vertically to place the different materials into the beam. We used two carbon foils of 0.54 and 0.76 mg/cm^2 thickness and a MgO foil of $\approx$2 mg/cm^2 for the measurements of the 4.438 MeV line shape. For γ-ray production on ^{24}Mg and Fe, we used an isotopically pure ^{24}Mg foil with thickness 1.58 mg/cm^2 and a 9.4 mg/cm^2 thick foil of natural iron, respectively. The foils were turned by 22.5° with respect to the normal of the beam direction.

For each proton and α-particle energy, the position and size of the beam spot were first controlled optically by means of the fluorescence of the MgO target. In addition to runs with the different targets which lasted typically 30 min, we also made runs for most beam energies with an empty frame to determine part of the beam-induced background. The beam intensity was measured in a Faraday cup which consisted of a 1.5 m long stainless steel vacuum tube electrically isolated from the target chamber and equipped with a thick copper disk downstream of the target in which the beam particles were stopped. This tube crossed a 75 cm thick concrete wall to shield the target chamber and detector area against the beam dump, thereby reducing the neutron and γ-ray flux from beam-induced reactions in the copper. Typical beam intensities were 3–15 nA. For each run, including the runs with an empty frame, we accumulated a typical charge of 2–10 μC and up to 30 μC for runs with the carbon target at low beam energies to obtain high-precision line profiles.

γ-rays were detected in five high-purity Ge detectors with bismuth germanate (BGO) scintillator shields for active Compton suppression from the Eurogam phase I setup [15].[1] The detectors were equipped with a 3.5 cm thick tungsten collimator of 5 cm diameter defining the detector solid angle and used to prevent direct x and γ rays from the target from reaching the BGO scintillators. A 3 mm thick copper disk was fixed in front of the collimator to reduce the count rate due to x rays and low-energy γ rays in the Ge crystals. The detectors were placed at a distance of 35 cm from the target and at angles of 45°, 67.5°, 90°, 135°, and 157.5° with respect to the beam direction. Because of the failure of one of the detectors during the experiment, there are no γ-ray data at 45° for some proton energies.

Data for 4.438 MeV line production in α-particle reactions were taken in energy steps of 1 MeV in the range 7.5–16 MeV and in steps of 2–5 MeV up to a maximum energy of 37.5 MeV. Proton reactions with carbon were measured in the energy ranges 5–8.4 and 20–25 MeV and with MgO in the range 20–25 MeV. These energies had not been covered in a previous experiment at the Orsay tandem [12]. The γ-ray production

[1]Provided by IN2P3-EPSRC French-UK Gamma-Ray Loan Pool (http://ipnweb.in2p3.fr/GePool/poolRules.html).

in reactions with proton beams onto ^{24}Mg and Fe targets was measured at five incident energies in the range 5–25 MeV and at seven incident energies ranging from 8.5 to 40 MeV with α-particle beams. Furthermore, we took data by irradiating the piece of meteorite with proton beams of 5, 10, 15, 20, and 25 MeV.

The Allende meteorite belongs to the class of carbonaceous chondrites and, with the exception of volatile elements, presents the same element abundances as the solar photosphere. The irradiated piece was thick enough to stop the proton beams, so the γ-ray spectra taken during and after its irradiation are valuable in testing the predicted total nuclear γ-ray emission in thick-target irradiation models of the solar atmosphere. These studies are under way. A typical spectrum from these irradiations is shown in Fig. 1, where the major γ-ray lines of the most abundant nuclei can be clearly identified.

Data for energy and efficiency calibration of the detectors were taken before, during, and after the proton and α-particle irradiation with calibrated sources of ^{60}Co, ^{137}Cs, and ^{152}Eu placed on the target holder. The detector efficiency remained constant over the experiment as expected, while some shifts in the energy response not exceeding 10 keV at 4 MeV were observed over the 1-week period of the experiment. Therefore we used also beam-induced γ-rays and lines from natural radioactivity for the energy calibration of spectra.

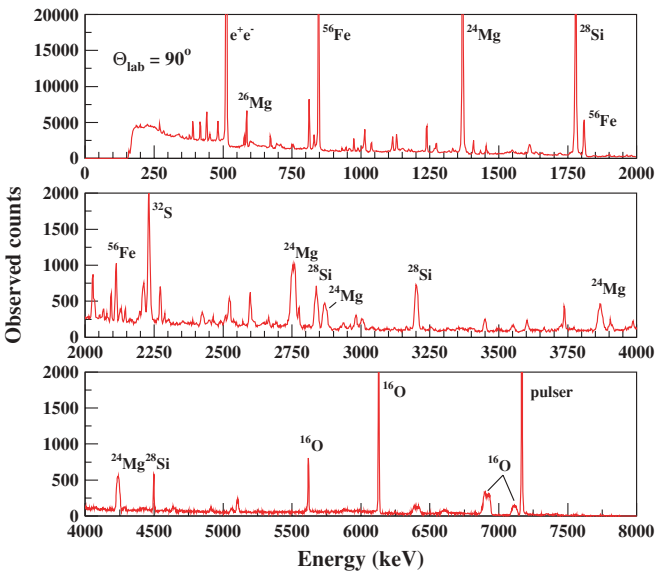

FIG. 1. (Color online) Compton-suppressed γ-ray spectrum obtained at 90° for a 10 MeV proton beam incident on the piece of the Allende meteorite. The emitting nuclei for some of the strongest lines are indicated. At this beam energy and with the exception of the positron annihilation line, the strongest lines are from inelastic scattering reactions off the most abundant isotopes in the meteorite material, namely, ^{16}O, ^{24}Mg, ^{28}Si, and ^{56}Fe. The large width of some lines is explained by Doppler broadening due to in-flight γ-ray emission from the recoiling excited nuclei. Very narrow lines such as the 6.129 MeV line of ^{16}O are from excited levels with lifetimes exceeding several hundreds of fs, for which the γ-ray emission takes place predominantly after stopping of the recoiling nucleus.

Conventional electronic and data acquisition techniques were used to translate the detector output signals into pulse-height spectra. We generated two spectra for each detector, a direct spectrum of events in the Ge crystals neglecting any veto signal from the BGO detectors, and a Compton-suppressed spectrum from anticoincidence events between Ge and BGO signals. The dead time of the system was precisely determined with a set of pulsers whose signals were fed into the Ge-detector preamplifiers and into a counter that was triggered by the data acquisition system. Typical data acquisition dead times were 5–20%.

III. DATA ANALYSIS

Differential cross-section data for a particular γ-ray transition were deduced from the corresponding line integrals in the spectra of the five detectors. Two procedures were used: a simple integration of line counts with subtraction of a background estimated from count levels below and above the peak, and a standard fitting procedure with parametrized response of Ge detectors to (practically) monoenergetic γ rays including a smooth background [16]. Both procedures were usually employed for narrow lines, giving an estimate of the uncertainty due to the background subtraction which was added quadratically to the statistical error. For broader lines, only the first method could be applied, and we assigned an uncertainty by estimating a maximal and a minimal background.

Some broad lines, however, received special treatment. The 4.438 MeV line profiles and their integrals were obtained by subtracting first the background level above the line and then the Compton events on a channel-by-channel basis, starting at the high-energy edge of the line. The line integrals determined in that way agreed well with the simpler procedure of a linear background interpolation between count rates below and above the lines, which was employed for most of the other broad lines.

In difficult cases in which the signal-to-background ratio was small or for complex structures of superimposed lines, we estimated the integrals with the help of simulated line shapes. A substantial uncertainty was then usually assigned to the result to take account of eventual errors in the subtraction of background or interfering lines. This concerned mostly relatively broad lines but also some narrow lines, particularly in runs with high-energy α particles on the ^{24}Mg and Fe targets, where a vast number of lines were produced in inelastic scattering, spallation, and fusion-evaporation reactions. At proton and α-particle energies above 20 MeV, background from secondary neutron interactions became important despite the shielding of the Faraday cup. However, interfering lines from neutron reactions could be subtracted in most cases using the runs with an empty frame.

The broad line of ^{20}Ne at 1.634 MeV, produced in the spallation of ^{24}Mg by α particles, also received a special treatment because it was completely merged with broad lines of ^{25}Al and ^{25}Mg at 1.612 MeV and ^{26}Al at 1.652 MeV from fusion-evaporation reactions and the spallation line of ^{23}Na at 1.636 MeV. Here we employed detailed simulations of the

γ-ray emission for each of the above mentioned lines. The background-subtracted lines of the five detectors were then fitted with the simulated line profiles leaving the intensities of the different simulated lines as free parameters. As the 1.634 and 1.636 MeV lines could not be separated, they were treated as a unique line. The uncertainty of the procedure was estimated by varying the parameters describing the nuclear reaction.

Most of the line integrals were obtained from the Compton-suppressed spectra, but we analyzed also direct spectra for some lines. No difference within the error bars could be observed when taking into account the acquisition dead times. These dead times were determined from the ratio of counts of the pulser lines in the γ-ray spectra and the counter. Compton-suppressed spectra were subject to slightly larger dead times than the direct spectra, which was probably due to accidental coincidences between events in the Ge detector and its corresponding BGO shield. This difference and the differences between individual detectors were used to estimate the uncertainty of the dead-time determination, usually in or below the 1% range.

The γ-ray fluxes at the different detector angles where then obtained with the dead-time-corrected line integrals. Full-energy peak efficiencies for the different detectors as a function of γ-ray energy were determined with the help of the three radioactive sources which were calibrated in activity to 2.5% and detailed Monte Carlo simulations of the detection setup with the GEANT-3 package [17]. It included the target-chamber walls, the W collimator and Cu plates and the exact Ge-crystal dimensions. These simulations were checked on experimental efficiency curves of several of the Eurogam phase I detectors which were obtained prior to our experiment with ^{152}Eu and ^{56}Co sources and the 992 keV resonance of ^{27}Al(p,γ), spanning the entire interesting energy range from about 250 keV to 10 MeV. We estimated an uncertainty smaller than 1.5% for the relative detector efficiencies.

All uncertainties mentioned above were then added, quadratically defining the total error bars of the γ-ray angular distribution data. The distributions were obtained from Legendre-polynomial fits to the data:

$$W(\Theta) = \sum_{l=0}^{l=l_{\max}} a_l Q_l P_l(\cos\Theta) \quad (l \text{ even}), \tag{1}$$

with $l_{\max}$ being twice the γ-ray transition multipolarity and Q_l the attenuation coefficients, which were calculated analytically for the actual detector setup (see, for example, Ref. [18]). The coefficient a_0 is directly proportional to the angle-integrated cross section. The reduced χ^2 of the fits stayed usually below unity, indicating that we slightly overestimated the uncertainties, most probably those assigned to the detection efficiency. Sometimes, however, especially for data in runs at the highest proton and α-particle energies, the χ^2 attained values above 2.0, probably due to interference of unobserved background lines. In such cases, we decided to increase the uncertainties of the background subtraction such that values for χ^2 around unity were obtained.

The areal densities of the carbon and ^{24}Mg targets were determined by Rutherford backscattering (RBS) measurements at ARAMIS, the 2-MV tandem Van-de-Graaff accelerator of the CSNSM Orsay. A narrow 1 mm diameter proton beam of 1.6 MeV and about 50 nA was directed on typically five different positions of each foil. During these measurements the ^{24}Mg target foil and the two carbon targets were mounted on a gold plate. In a second measurement, we mounted the carbon targets on aluminum plates which allowed an improved determination of the densities of the carbon foil compared to the gold backing. The backscattered protons were detected in a surface-barrier Si detector placed at 165° to the beam direction. The target density was obtained by analyzing the spectra of backscattered protons with standard RBS analyzing tools [19,20] and with the computer code SRIM [21]. The density of the Fe target was obtained by weighing the foil with a precision balance.

The areal density of the MgO target consisting of a MgO deposit on a thin Al foil could not be determined in the RBS measurements because of pronounced inhomogeneities of the deposit. We determined the effective oxygen densities for each run separately by normalizing the measured 4.438 and 6.129 MeV line fluxes relative to the data of Refs. [22,23] for proton and α-particle reactions. The effective magnesium densities were inferred from the yields of the lines at 0.440 and 0.451 MeV from ^{23}Na and ^{23}Mg, respectively.

These two lines are relatively strong and predominantly produced with α particles by spallation of ^{24}Mg, the production by spallation of other magnesium isotopes or ^{27}Al being weak because of high thresholds or small branching ratios. The cross sections for the production of these two lines by spallation of ^{24}Mg were taken from this experiment, obtained in runs with the ^{24}Mg target. For proton bombardment, we used only the ^{23}Mg line for the areal density determination, because ^{23}Na in the MgO target is also strongly produced by the ^{26}Mg(p,α) reaction and by proton induced spallation of ^{27}Al. The oxygen-to-magnesium ratios obtained with this method and with the RBS measurements were all compatible with the stoichiometry of pure MgO.

IV. RESULTS

One of the aims of the present experiment was to increase the existing database of γ-ray production cross sections. Most of the existing cross-section excitation functions were obtained at the University of Washington tandem Van-de-Graaff accelerator [22–24]. Other relevant cross sections can be found in Refs. [25–27]. In general, these studies concentrated on the strongest γ rays from transitions from the first few excited states in the target nucleus and in some residual nuclei. In our analysis, we could extract data for many more transitions including from higher lying levels, especially in reactions with the ^{24}Mg and the Fe targets. Lists of about 100 cross-section excitation functions which we obtained are presented in Tables I–VI, together with previous measurements which came to our knowledge. We did not include the data of Zobel *et al.* [29], because their cross sections are often incompatible with other literature values; the reasons for these discrepancies are understood [27]. In the following, most of our comparisons are done with the γ-ray data from the University

TABLE I. Measured γ-ray production cross-section excitation functions for protons and α particles incident on the carbon target. Listed are the emitting nucleus, initial and final state energies of the γ-ray transition, and measured beam energy range. Level energies are from Ref. [28]. The two last columns listed all previous measurements of γ-ray production cross sections with their beam energy ranges which came to our knowledge (with the exception of Zobel *et al.* [29], see text). The energy ranges are from the published tabulated values in Lang *et al.* [26], Lesko *et al.* [25], Narayanaswamy *et al.* [27], and from original material in Kiener *et al.* [12]. For references Dyer1 *et al.* [22], Dyer2 *et al.* [23], Seamster *et al.* [24], energy values were extracted from the figures with cross-section excitation functions (corrected for energy loss in the target) with an estimated uncertainty of 0.1 MeV.

Reaction	Em. nucleus	$E_i \rightarrow E_f$ (keV)	E_{beam} (MeV)	Other data	E_{beam} (MeV)
$p + \text{C}$	^{12}C	4438.91 → g.s.	5.0–8.4; 20–25	Dyer1 *et al.*	5.1–23.0
				Lang *et al.*	40–85
				Lesko *et al.*	8.895–50.0
				Kiener *et al.*	8.4–19.75
$\alpha + \text{C}$	^{15}N[a]	5270.155 → g.s.	17.5–37.5		
	^{14}N[b]	2312.798 → g.s.	18.0–37.5		
	^{14}N	5105.89 → g.s.	32.5–37.5		
	^{12}C	4438.91 → g.s.	7.5–37.5	Dyer2 *et al.*	7.7–27.0

[a]Composite line, other transitions: ^{15}N 5298.822 → g.s.; ^{15}O 5183 → g.s.; ^{15}O 5240.9 → g.s.
[b]Composite line, other transition: ^{15}N 7567.1 → 5240.9.

of Washington laboratory, and we will refer to them as the Washington data. Numerical values of our results can be found in the appendix.

A. The 4.438 MeV line

The line is from the deexcitation of the first excited state of ^{12}C, 2^+ 4.439 MeV, which is the only particle-bound excited state in ^{12}C. This means in particular that there is negligible feeding from higher excited states, which simplifies considerably the nuclear reaction calculations of the excited-state population and the subsequent γ-ray emission compared to other strong interaction lines [13]. These calculations, however, need to be compared with experimental line profiles, especially at low energies where both compound-nucleus resonances and the direct excitation mechanism contribute substantially to the line production.

Line profiles for projectile energies below 20 MeV could be obtained from the spectra by simply subtracting background

TABLE II. Same as Table I, except for proton and α particles incident on the MgO target.

Reaction	Em. nucleus	$E_i \rightarrow E_f$ (keV)	E_{beam} (MeV)	Other data	E_{beam} (MeV)
$p + \text{MgO}$	^{26}Mg	1808.70 → g.s.	20.0–25.0		
	^{26}Mg	2938.38 → 1808.70	20.0–25.0		
	^{25}Mg	585.04 → g.s.	20.0–25.0		
	^{16}O	6129.89 → g.s.	20.0–25.0	Dyer1 *et al.*	7.3–23.0
				Lang *et al.*	40–85
				Lesko *et al.*	8.895–50.0
				Kiener *et al.*	8.4–19.75
				Narayanaswamy *et al.*	23.7; 44.6
	^{15}N[a]	5270.155 → g.s.	20.0–25.0	Lang *et al.*[b]	40–85
				Lesko *et al.*[b]	30.0–40.0
	^{12}C	4438.91 → g.s.	20.0–25.0	Dyer1 *et al.*	15.4–23.0
				Lang *et al.*	40.0
				Lesko *et al.*	20.0–50.0
$\alpha + \text{MgO}$	^{16}O	6129.89 → g.s.	20.0–37.5	Dyer2 *et al.*	10.2–27.0[c]
	^{16}O	6917.1 → g.s.	20.0–27.5	Dyer2 *et al.*	11.8–27.0[c]
	^{16}O	7116.85 → g.s.	20.0–27.5	Dyer2 *et al.*	11.8–27.0[c]
	^{15}N[a]	5270.155 → g.s.	32.5–37.5		
	^{12}C	4438.91 → g.s.	20.0–37.5	Dyer2 *et al.*	21.7–27.0

[a]Composite line, see Table I.
[b]Cross sections of ^{15}N 5270.155 → g.s. and ^{15}O 5240.9 → g.s. separately.
[c]Corrected for an apparent discrepancy of 0.3 MeV between energy values extracted from Fig. 5 and those given in Table 1 in Dyer2 *et al.*

TABLE III. Same as Table I, except for protons incident on the ^{24}Mg target.

Reaction	Em. nucleus	$E_i \rightarrow E_f$ (keV)	E_{beam} (MeV)	Other data	E_{beam} (MeV)
$p + {}^{24}$Mg	^{24}Al	425.8 → g.s.	20.0		
	^{24}Mg	1368.675 → g.s.	5.0–25.0	Dyer1 *et al.*	2.3–23.0
	^{24}Mg	4122.874 → 1368.675	5.0–25.0		
	^{24}Mg	4238.36 → g.s.	10.0–25.0		
	^{24}Mg	5235.20 → 1368.675	10.0–25.0		
	^{24}Mg	6010.32 → 1368.675	10.0–25.0		
	^{24}Mg	6432.5 → 1368.675	10.0; 15.0		
	^{24}Mg	7349.05 → g.s.	10.0–20.0		
	^{24}Mg	7555.3 → g.s.	10.0		
	^{24}Mg	7555.3 → 1368.675	10.0–20.0		
	^{24}Mg	7555.3 → 4238.36	10.0; 15.0		
	^{24}Mg	7616.47 → 1368.675	10.0–25.0		
	^{23}Mg	450.70 → g.s.	20.0; 25.0		
	^{23}Na	439.991 → g.s.	15.0–25.0		
	^{23}Na	2703.50 → 439.991	20.0; 25.0		
	^{21}Na	331.93 → g.s.	10.0–25.0		
	^{21}Na	β-decay	15.0; 20.0		
	^{20}Ne[a]	1633.674 → g.s.	20.0; 25.0	Dyer1 *et al.*	15.7–24.0
	^{20}Ne	4247.7 → 1633.674	20.0; 25.0		
	^{20}Ne	4966.51 → g.s.	20.0; 25.0		

[a]Composite line, other transition: ^{23}Na 2076.01 → 439.991.

components as explained above. At higher energies, however, two background lines of unknown origin, one at 4.422 MeV and the escape peak of a line at 4.937 MeV, were overlapping with the 4.438 MeV line, requiring subtraction of spectra taken with an empty frame. We noticed also a small amount of oxygen in the carbon target. This was already observed in other experiments and attributed to water contamination of the carbon foils [30]. The oxygen density was deduced from the intensity of the 6.129 MeV line and was ≈70 μg/cm^2 during the first runs with α-particle beams. It diminished in the course of the irradiations and was undetectable in the runs with proton beams. The contribution of ^{16}O spallation to the 4.438 MeV line was subtracted for runs with α particles incident on carbon at energies above 22.5 MeV. In the case of the MgO target, we subtracted spectra taken with the ^{24}Mg target.

For all runs with carbon targets, we obtained a minimum of 5000 counts in the line and 3500 counts with the MgO target, resulting in high-accuracy line profiles with very good statistics at low beam energies where the background was low and essentially only from Compton-scattered events of 4.4 MeV photons. At the highest energies, the line-to-background ratio dropped in some spectra to values smaller than unity, especially for the detector at 135°, where the Compton-suppressed spectra could not be used for most of the runs, and at 45°, where the neutron induced background was maximal. Typical examples of measured line profiles for α-particle beams on the carbon target are shown in Fig. 2.

For the γ-ray production cross sections obtained with the carbon and MgO targets, we ignore in the following the contribution of reactions with the isotopes ^{13}C, ^{17}O, and ^{18}O, which have small isotopic abundances of 1.1%, 0.038%, and 0.20%, respectively. We attribute the analyzed γ-ray lines entirely to reactions with the main isotopes ^{12}C and ^{16}O, which in any case introduces an error completely negligible with respect to the other uncertainties.

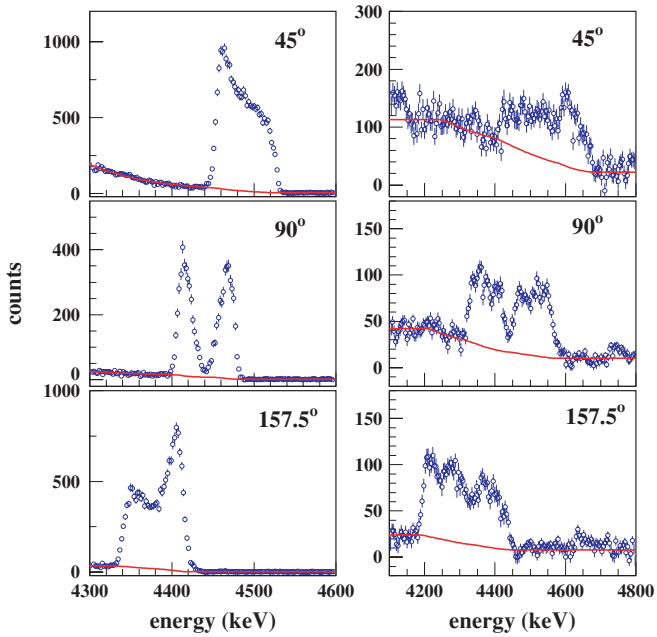

FIG. 2. (Color online) Details of measured spectra around the 4.438 MeV line for two runs with α-particle beams of 8 (left) and 30 MeV (right) incident on the carbon target. The spectra at E_α = 30 MeV were obtained after subtraction of spectra taken with an empty frame, normalized to the same integrated beam charge. Continuous lines show the adopted background which was subtracted to obtain the line shapes.

TABLE IV. Same as Table I, except for α particles incident on the ^{24}Mg target.

Reaction	Em. nucleus	$E_i \rightarrow E_f$ (keV)	E_{beam} (MeV)	Other data	E_{beam} (MeV)
$\alpha + {}^{24}$Mg	^{27}Si	780.9 → g.s.	15.0–30.0		
	^{27}Si	780.9 → g.s.	15.0–30.0		
	^{27}Si	2163.6 → g.s.	15.0–25.0		
	^{27}Al	843.76 → g.s.	8.5–40.0		
	^{27}Al	1014.45 → g.s.	8.5–40.0		
	^{27}Al	2211.1 → g.s.	8.5–40.0	Seamster *et al.*	7.0–27.0
	^{27}Al	2734.9 → 1014.45	8.5–25.0		
	^{27}Al[a]	3004.2 → g.s.	8.5–40.0		
	^{27}Al	3004.2 → 2111.1	8.5–40.0		
	^{27}Al	3680.4 → 1014.45	8.5–25.0		
	^{27}Al	3956.8 → g.s.	8.5		
	^{27}Al	4054.6 → 843.76	8.5–25.0		
	^{27}Al	4510.3 → 3004.2	8.5–30.0		
	^{27}Al	4510.3 → 2211.1	8.5–25.0		
	^{26}Al	416.852 → g.s.	20.0–40.0		
	^{26}Al	2068.86 → g.s.	25.0–35.0		
	^{26}Mg	1808.70 → g.s.	20.0–40.0		
	^{26}Mg	2938.38 → 1808.70	20.0–40.0		
	^{25}Mg	585.04 → g.s.	25.0–40.0		
	^{25}Mg	974.74 → 585.04	35.0; 40.0		
	^{24}Mg	1368.675 → g.s.	8.5–40.0	Seamster *et al.*	7.0–27.0
	^{24}Mg	4122.874 → 1368.675	8.5–30.0		
	^{24}Mg	4238.36 → g.s.	8.5; 15.0		
	^{24}Mg	5235.20 → 1368.675	15.0–25.0		
	^{24}Mg	6010.32 → 1368.675	15.0–30.0		
	^{23}Mg	450.70 → g.s.	30.0–40.0		
	^{23}Na	439.991 → g.s.	20.0–40.0		
	^{20}Ne[b]	1633.674 → g.s.	20.0–40.0	Seamster *et al.*	20.5–27.0
	^{20}Ne[c]	1633.674 → g.s.	25.0–40.0		

[a]Composite line, other transition: ^{27}Al 2082.0 → g.s.
[b]Composite line, other transition: ^{23}Na 2076.01 → 439.991.
[c]Composite line, other transitions: ^{23}Na 2076.01 → 439.991; ^{26}Al 2068.86 → 416.852; ^{25}Mg 1611.767 → g.s.

The cross-section excitation functions for proton and α-particle reactions with ^{12}C and ^{16}O are shown in Fig. 3. Error bars reflect the fit errors of a_0 in the Legendre polynomial fits to the γ-ray angular distribution data. They contain thereby implicitly statistical uncertainties, estimated errors for dead-time correction, background subtraction, and detector efficiencies. To these should be added an overall uncertainty in the cross-section normalization, which is estimated to be less than 10% for data taken with the carbon targets and 15% with the MgO target. It includes uncertainties in the target thickness ($\approx$7% for the two carbon targets and $\approx$15% for the MgO target), beam charge determination (2.5%), and absolute detector efficiencies (2.5%). Within uncertainties, there is very good agreement between our data and the Washington data [22,23].

B. Other lines with ^{12}C and ^{16}O target nuclei

In addition to the 4.438 MeV line, we also extracted cross sections for other strong lines produced in proton and α-particle reactions with ^{12}C and ^{16}O. These are the 6.129, 6.916, and 7.116 MeV lines emitted after inelastic scattering reactions off ^{16}O; the line complex containing the 2.313 and 2.297 MeV lines of ^{14}N and ^{15}N, respectively; and the broad bump around 5.2 MeV, composed of several lines of ^{15}N and ^{15}O and the 5.105 line of ^{14}N. Those lines were produced in

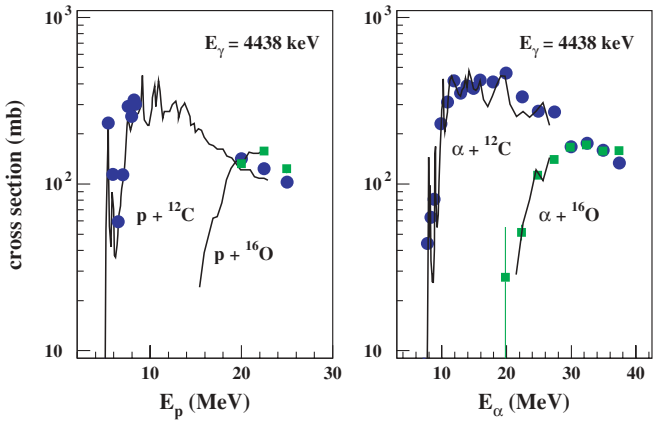

FIG. 3. (Color online) Cross-section excitation functions for the 4.438 MeV γ-ray production in reactions of protons (left) and α particles (right) with ^{12}C and ^{16}O. Filled symbols: data from this experiment; when error bars are not visible they are smaller than the symbol size. Solid lines: Washington data.

TABLE V. Same as Table I, except for protons incident on the Fe target.

Reaction	Em. nucleus	$E_i \rightarrow E_f$ (keV)	E_{beam} (MeV)	Other data	E_{beam} (MeV)
p + Fe	^{56}Co	970.23 → 158.38	5.0–20.0	Dyer1 *et al.*[a]	6.6–23.0
	^{56}Co	1450.68 → 970.23	5.0–25.0		
	^{56}Fe[b]	846.776 → g.s.	5.0–25.0	Dyer1 *et al.*[a]	4.5–23.0
				Lesko *et al.*	8.895–50.0
	^{56}Fe	2085.076 → 846.776	5.0–25.0	Dyer1 *et al.*[a]	5.0–23.0
				Lesko *et al.*	8.895–50.0
	^{56}Fe	2657.562 → 846.776	5.0–20.0	Dyer1 *et al.*[a]	4.7–22.0
	^{56}Fe	2941.7 → 846.776	5.0–20.0		
	^{56}Fe	2959.923 → 846.776	5.0–20.0		
	^{56}Fe	3119.6 → 846.776	5.0–20.0		
	^{56}Fe	3122.927 → 2085.076	5.0–25.0		
	^{55}Fe	411.42 → g.s.	15.0–25.0		
	^{55}Fe	931.29 → g.s.	5.0–25.0	Dyer1 *et al.*[a]	14.9–23.0
				Lesko *et al.*	20.0–50.0
	^{55}Fe	1316.54 → g.s.	10.0–25.0	Dyer1 *et al.*	15.5–23.0
				Lesko *et al.*	20.0–50.0
	^{55}Fe[c]	1408.45 → g.s.	5.0–25.0	Lesko *et al.*	8.895–50.0
	^{55}Mn	125.949 → g.s.	20.0; 25.0		
	^{54}Fe	2538.1 → 1408.19	5.0–15.0	Lesko *et al.*	8.895–50.0
	^{52}Cr	1434.090 → g.s.	20.0; 25.0	Lesko *et al.*	8.895–40.0

[a]Data taken with isotopically enriched ^{56}Fe target.
[b]Composite line, other transitions see text.
[c]Composite line, other transition: ^{54}Fe 1408.19 → g.s.

the spallation of ^{16}O and in fusion-evaporation reactions of α particles with ^{12}C. Other lines from the bombardment of ^{12}C and ^{16}O were too weak or superimposed with lines from reactions with magnesium isotopes or ^{27}Al as, for example, the relatively strong 2.742 MeV line of ^{16}O.

Cross sections for the 6.129 MeV line could be obtained for proton and α-particle inelastic scattering at all projectile energies, while 6.916 and 7.116 MeV line cross sections could only be extracted for runs with α particles in the energy range 20–30 MeV. At higher energies, the lines got weaker and too broad to permit a reasonable subtraction of the underlying background. For the three runs with proton beams at 20, 22.5, and 25 MeV, neutron-capture lines were seriously interfering, and we estimated it as not being worthwhile to extract cross sections with probably large uncertainties while data exist up to 23 MeV [22]. Our measured cross sections for inelastic α-particle scattering off ^{16}O are shown in Fig. 4 together with Washington data [23]. There is reasonable agreement between both data sets in the overlap energy range $E_\alpha = 20$–25 MeV.

The structure at 2.3 MeV could be unambiguously seen in the spectra of α-particle beams incident on carbon targets at energies above 18 MeV. Although the two lines could not be separated, one can infer from the line centroid that the structure is clearly dominated at energies below $E \simeq 25$ MeV by the γ ray from the $7/2^+$ 7.567 MeV → $5/2^+$ 5.270 MeV transition in ^{15}N following the ^{12}C(α, p)^{15}N reaction, whose reaction threshold is 16.7 MeV in the laboratory. Above 25 MeV, the ^{12}C(α, pn)^{14}N reaction inducing the 2.313 MeV γ ray from the first excited state of ^{14}N with a threshold of 24.2 MeV [21.2 MeV for (α, d)] starts to contribute and gets dominant at the highest energies. Only the detectors at 45°, 67.5°, and 90° were used for analysis, because the structure overlapped with the 2.223 MeV neutron-capture line from ^{1}H(n, γ)^{2}H in the spectra of the two backward-angle detectors.

The thresholds for the 2.296 and 2.313 MeV line production in spallation reactions of ^{16}O are, respectively, 24.6 and 31.6 MeV. There is clear indication of the 2.296 MeV line in the spectra of α-particle bombardment of MgO above $E_\alpha = 30$ MeV, but completely merged with other relatively strong lines, certainly from reactions with Mg isotopes. It seemed impossible to obtain reasonable line integrals from the

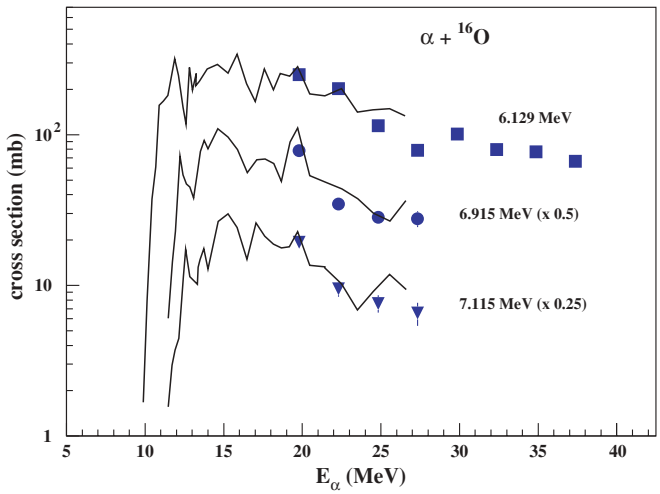

FIG. 4. (Color online) Cross-section excitation functions for ^{16}O lines produced in α-particle inelastic scattering. Symbols and lines as in Fig. 3.

TABLE VI. Same as Table I, except for α particles incident on the Fe target.

Reaction	Em. nucleus	$E_i \rightarrow E_f$ (keV)	E_{beam} (MeV)	Other data	E_{beam} (MeV)
α + Fe	^{59}Ni	339.421 → g.s.	8.5–40.0		
	^{59}Ni[b]	1188.82 → g.s.	8.5–40.0	Seamster *et al.*[a]	8.5–27.0
	^{59}Ni[c]	1301.409 → g.s.	8.5–40.0		
	^{59}Ni[d]	1337.89 → g.s.	8.5–25.0		
	^{59}Ni[e]	1337.89 → 339.421	8.5–40.0	Seamster *et al.*[a]	8.1–27.0
	^{59}Ni	1767.45 → 339.421	8.5–30.0		
	^{59}Ni	2705.02 → 1337.89	15.0–30.0	Seamster *et al.*[a]	10.0–26.0
	^{59}Ni	3054.33 → 1947.93	15.0–25.0		
	^{59}Co	1099.262 → g.s.	8.5–25.0		
	^{59}Co[f]	1459.52 → g.s.	15.0–40.0	Seamster *et al.*[a]	12.0–27.0
	^{58}Ni	1454.45 → g.s.	20.0–40.0		
	^{58}Co[g]	1049.36 → g.s.	20.0–40.0	Seamster *et al.*[a]	19.1–27.0
	^{58}Co	1049.36 → 111.52	20.0–40.0		
	^{58}Co[h]	1424.9 → 24.889	20.0–40.0		
	^{56}Fe[i]	846.776 → g.s.	8.5–40.0	Seamster *et al.*[a]	7.6–27.0
	^{56}Fe[j]	2085.076 → 846.776	8.5–40.0	Seamster *et al.*[a]	12.0–27.0
	^{56}Fe	2657.962 → 846.776	8.5–30.0		
	^{56}Fe[k]	2941.7 → 846.776	8.5–25.0		
	^{56}Fe	3122.927 → 2085.076	8.5–30.0		
	^{56}Fe	2959.923 → 846.776	5.0–20.0		
	^{55}Fe	931.29 → g.s.	25.0–40.0		

[a]Data taken with isotopically enriched ^{56}Fe target above $E_\alpha = 10.5$ MeV.
[b]Composite line, other transition: ^{59}Co 1190.45 → g.s.
[c]Composite line, other transition: ^{56}Fe 3388.49 → 2085.076.
[d]Composite line, other transitions: ^{59}Ni 1679.704 → 339.421; ^{60}Ni 1332.516 → g.s.; ^{56}Fe 4458.532 → 3122.927.
[e]Composite line, other transitions: ^{59}Co 2183.5 → 1190.45; ^{58}Ni 2459.1 → 1454.45.
[f]Composite line, other transition: ^{58}Ni 1454.45 → g.s.
[g]Composite line, other transition: ^{58}Co 1424.9 → 373.9.
[h]Composite line, other transition: ^{59}Ni 1739.24 → 339.421.
[i]Composite line, see text.
[j]Composite line, other transition: ^{58}Co 1236.5 → g.s.
[k]Composite line, other transition: ^{56}Fe 2959.923 → 847.776.

spectra. No indication of the 2.313 MeV line in these spectra could be found.

The broad line structure at 5.2 MeV is nicely seen for α-particle reactions with the carbon target above 15 MeV. The four principal lines are from ground-state transitions of the first two excited states of ^{15}N, $5/2^+$ 5.270 MeV and $1/2^+$ 5.299 MeV, and their mirrors in ^{15}O, $5/2^+$ 5.241 MeV and $1/2^+$ 5.183 MeV. Thresholds are $E_\alpha^{\text{lab}} \simeq 14$ and 18 MeV for the lines of ^{15}N and ^{15}O from the reactions ^{12}C(α, p)^{15}N and ^{12}C(α, n)^{15}O, respectively. Line centroids and widths are consistent with a pure contribution of the ^{15}N lines below 20 MeV and slowly increasing contribution of ^{15}O lines above.

Proton spallation of ^{16}O produces these lines with reaction thresholds of 18.5 and 22.2 MeV for the lines of ^{15}N and ^{15}O, respectively. The 5.2 MeV structure is clearly present for proton energies of 22.5 and 25 MeV. It appears dominated by the 5.241 and 5.270 MeV lines, while the lines at 5.183 and 5.299 are much weaker and barely visible in the spectra. The thresholds for α-particle induced spallation of ^{16}O are about 3 MeV higher, but we could extract cross sections only at $E_\alpha^{\text{lab}} = 32.5$–$37.5$ MeV.

Finally, the 5.105 MeV line from the ground-state transition of the 2^- 5.106 MeV state of ^{14}N was distinguishable for α-particle reactions with carbon at the three highest α-particle energies. The 5.106 MeV γ-ray production threshold for the ^{12}C(α, pn)^{14}N reaction is $E_\alpha^{\text{lab}} = 27.9$ MeV [24.9 MeV for (α, d)].

Spallation and fusion-evaporation γ-ray data are shown in Fig. 5. There are no literature data to compare against in this energy range. Lesko *et al.* [25] measured the cross sections for ^{16}O(p, $pn\gamma_{5.240}$)^{15}O and ^{16}O(p, $2p\gamma_{5.269}$)^{15}N at 30, 33, and 40 MeV. The sum of both lines amounts to about 40 mb at 30 and 33 MeV. This is comparable to 37 mb, which we obtained at 25 MeV for the 5.2 MeV structure.

It is noteworthy that the higher cross sections and lower energy thresholds for α-particle reactions when expressed in energy per nucleon, in particular for ^{12}C(α, $p\gamma$)^{15}N indicate that the 5.2 MeV line compound may be predominantly produced by accelerated α particles in solar flares with soft particle spectra.

C. ^{24}Mg and Fe targets

We aimed at extracting cross sections of as many lines as possible for these two targets to provide a solid data

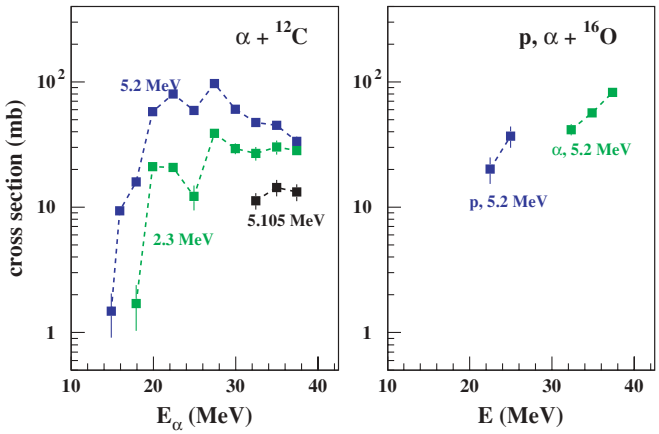

FIG. 5. (Color online) Cross-section excitation functions of γ-ray lines produced in fusion-evaporation reactions of α particles with ^{12}C (left) and in spallation reactions with ^{16}O (right). Dashed lines are to guide the eye.

base for tests of nuclear reaction calculations. Sensitivities were at or even below the 1 mb level for narrow lines produced in runs with proton or α-particle beams at low energy and deteriorated to approximately 10 mb for broad lines produced in particular at higher beam energies. This allowed us to obtain cross-section excitation functions for typically 25 γ-ray lines for each reaction.

1. *Lines from p + ^{24}Mg*

For proton inelastic scattering off ^{24}Mg we obtained cross-section data for 12 deexcitation lines from excited states up to the 7.616 MeV 3^- level. While at 5 MeV, only lines of the two first excited states at 1.369 and 4.123 MeV could be observed; all states up to the 7.616 MeV level were already observed at 10 MeV proton energy. For higher proton energies, line integration became more difficult, and cross-section data could not be extracted for several lines which could be easily analyzed at 10 MeV. As in the case for lines with the carbon and MgO targets, only error bars resulting from the Legendre polynomial fits are plotted. The overall uncertainty in the cross-section normalization is estimated to be less than 10% for data taken with the ^{24}Mg target.

Lines from proton induced spallation of ^{24}Mg were observed above 15 MeV, mainly from the residual nuclei ^{20}Ne (1.634, 2.614, 3.333 MeV), ^{23}Na (0.440, 1.636, 2.264 MeV) and ^{23}Mg (0.451, 1.600 MeV). We observed furthermore the 0.332 MeV line of ^{21}Na, produced at the measured energies by the ^{24}Mg$(p,\alpha\gamma)^{21}$Na reaction, the β-decay line of ^{21}Na at 0.351 MeV, and finally a weak line at 0.426 MeV, probably of ^{24}Al from ^{24}Mg$(p,n\gamma)^{24}$Al at $E_p = 20$ MeV. The 1.634 MeV line is attributed to ^{20}Ne but contains also the 1.636 MeV line of ^{23}Na, which could not be separated in the line analysis. As this 1.636 MeV line populates the 0.440 MeV level, an upper limit of its contribution can be inferred from the cross section of the 0.440 MeV line.

Excitation functions of nine inelastic scattering lines, representing the strongest transitions of the first nine excited states in ^{24}Mg (except for the 6.186 MeV line from the transition 1^- 7.555 $\rightarrow$ 2^+ 1.369 MeV which is weaker than the ground-state transition), are plotted in the left part of Fig. 6. These data can only be compared with the 1.369 MeV line data of the Washington experiment [22] where the cross section was measured between threshold and 23 MeV. Within the uncertainties, the agreement is excellent.

All of the excited states above the 1.369 MeV level for which we could observe at least one deexcitation line have a branching to this level, and in most cases it is the dominant transition. When summing up their feeding of the 1.369 MeV level, it amounts to approximately 50% of the 1.369 MeV cross section above $E_p = 10$ MeV. The direct population of the 1.369 MeV level by inelastic scattering can be inferred from the differential cross-section data of Crawley and Garvey [31] and Hassell *et al.* [32]. It amounts to $\approx$140 mb at $E_p =$ 17 MeV, $\approx$100 mb at $E_p = 20$ MeV, and $\approx$90 mb at $E_p =$ 25 MeV. This leaves about 50–60 mb of the 1.369 MeV γ-ray

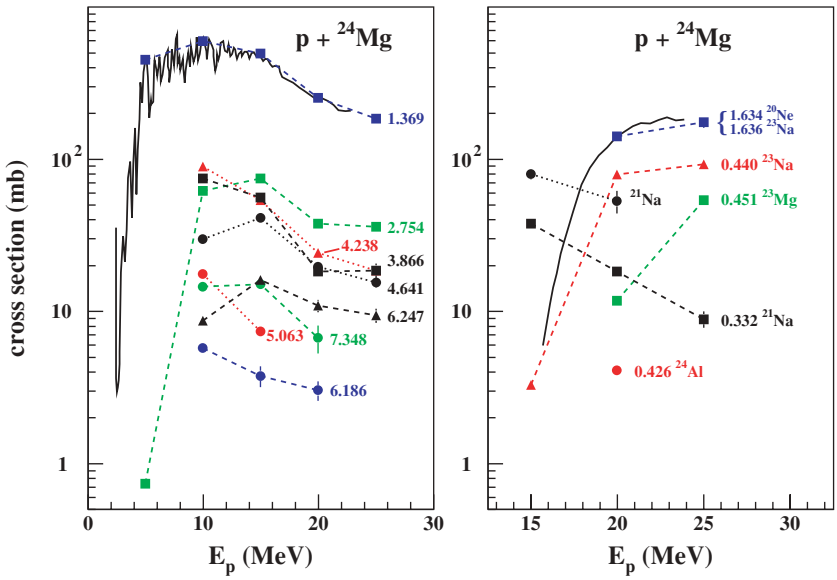

FIG. 6. (Color online) Cross-section excitation functions of γ-ray lines produced in inelastic scattering reactions of protons with ^{24}Mg (left) and in spallation, (p,α), and (p,n) reactions with ^{24}Mg (right). Dashed and dotted lines are to guide the eye. The continuous lines show the Washington data for the 1.369 MeV line produced by inelastic scattering (left) and for the feature composed of the 1.634 MeV ^{20}Ne and 1.636 MeV ^{23}Na spallation lines (right). The curves are labeled with the γ-ray line energy and the emitting nucleus. The label ^{21}Na designates the total production of this nucleus determined from its β^+ decay.

production cross section at $E_p = 17$ and 20 MeV and about 10 mb at $E_p = 25$ MeV to be shared by β^+ decay of ^{24}Al to the 1.369 MeV level and by feeding from unobserved transitions of higher lying levels.

Cross sections for the strongest lines from ^{24}Mg spallation in the different residual nuclei and lines from (p, α) and (p, n) reactions are presented in the right part of Fig. 6. Furthermore, the total production cross section of ^{21}Na ($t_{1/2} = 22.49$ s), deduced from its β^+-decay γ-ray line at 0.351 MeV is shown on the figure with fairly high values approaching 100 mb below $E_p = 20$ MeV. The highest cross sections are attained for the 1.634 MeV spallation line of ^{20}Ne, which shows very good agreement with the Washington data. Above 20 MeV, spallation to the residual nuclei ^{23}Na and ^{23}Mg becomes important, with cross sections for the 0.440 and 0.451 MeV γ-ray lines in the 50–100 mb range.

2. *Lines from $\alpha + ^{24}$Mg*

This projectile-target combination produces a fairly high number of γ-ray lines already at the lowest beam energies of 8.5 and 15 MeV, with an important contribution of fusion-evaporation reactions to the residual nucleus ^{27}Al. At higher energies, other residual nuclei such as ^{27}Si, ^{26}Al, and ^{26}Mg and spallation reactions to ^{20}Ne, ^{23}Na, and ^{23}Mg become increasingly important. For inelastic scattering, we extracted cross-section excitation functions for the strongest transitions of the five lowest lying excited states in ^{24}Mg. We obtained data up to the highest α-particle energy, however, only for the 1.369 MeV line; the other lines were too broad and too weak or contaminated with other lines, preventing reasonable determination of line integrals at the highest energies.

The cross sections for the lines produced by inelastic scattering are shown in Fig. 7 together with the Washington data [24], where the 1.369 MeV cross section was measured from threshold to 27 MeV. Both data sets are in reasonable agreement, though there is a 10–15% difference in absolute scale, which is at the limit of the estimated 10% uncertainty of both data sets.

A total of 20 different γ-ray lines from fusion-evaporation reactions could be analyzed, the emitting nuclei being ^{27}Al (11 lines), ^{27}Si (2), ^{26}Al (3), ^{26}Mg (2), and ^{25}Mg (2). For α-particle induced spallation of ^{24}Mg, we obtained data for the sum of the 1.634 MeV line of ^{20}Ne and the 1.636 MeV line of ^{23}Na, the 0.440 MeV line of ^{23}Na, and the 0.451 MeV of ^{23}Mg. Cross sections of the strongest lines are presented in Fig. 7 together with the Washington data for the 1.634 MeV line of ^{20}Ne (+ 1.636 MeV ^{23}Na) and the 2.211 MeV line of ^{27}Al [24]. The same reasonable agreement as for the 1.369 MeV line can be observed between both data sets.

The fusion-evaporation reactions are clearly dominated below $E_\alpha = 20$ MeV by the (α, p) reaction to ^{27}Al, the other one-nucleon evaporation reaction to ^{27}Si being much weaker, reflecting certainly the much higher threshold of the compound nucleus ^{28}Si for neutron (17.2 MeV) than for proton emission (11.6 MeV). Two-nucleon evaporation reactions and spallation to ^{20}Ne and ^{23}Na become important above $E_\alpha = 20$ MeV. The one-neutron spallation reaction to ^{23}Mg is much weaker, probably again because of the higher neutron-separation threshold of ^{24}Mg.

3. *Lines from p + Fe*

Having employed in this case an iron target foil with natural isotopic composition, a distinction between lines produced by inelastic scattering, (p, n), (p, α), or spallation reactions could not be made in general. The isotopes heavier than the most abundant one (^{56}Fe 91.75%), ^{57}Fe and ^{58}Fe have abundances of only 2.12% and 0.28%, which, summed together is a factor of $\approx$40 less than ^{56}Fe. Lines issue from transitions in ^{56}Fe are thus predominantly produced by inelastic scattering even above the one- or two-neutron separation threshold of ^{57}Fe and ^{58}Fe. However, all cross sections are calculated for consistency with an areal number density of Fe atoms including the four

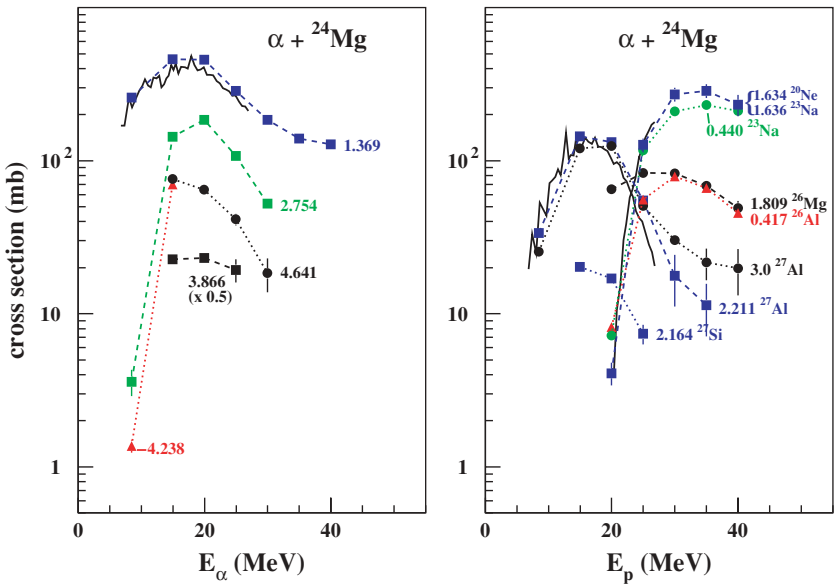

FIG. 7. (Color online) Cross-section excitation functions of γ-ray lines produced in inelastic scattering reactions of α particles with ^{24}Mg (left) and in spallation and fusion-evaporation reactions with ^{24}Mg (right). Dashed and dotted lines are to guide the eye. The continuous lines show the Washington data for the 1.369 MeV line produced by inelastic scattering (left), for the 1.634 MeV ^{20}Ne, 1.636 MeV ^{23}Na spallation line feature, and the 2.211 MeV line of ^{27}Al (right). The curves are labeled with the γ-ray line energy and the emitting nucleus. The curve labeled 3.0 ^{27}Al represents the sum of the cross sections of the 2.982 and 3.004 MeV lines.

stable Fe isotopes. The systematic overall uncertainty due to beam charge integration and target thickness uncertainties on the cross-section functions is estimated to be less than 5% for the Fe target.

We extracted cross-section excitation functions for seven lines produced predominantly by inelastic scattering off ^{56}Fe. They represent the strongest transitions of the first eight excited states of ^{56}Fe with the exception of the (3^-) 3.07 MeV level, whose decay properties are not known. The line integrals of the 0.847 MeV line from the deexcitation of the first excited state of ^{56}Fe were corrected for contribution of the 0.843 MeV line of ^{27}Al. The latter one was produced by inelastic scattering of secondary neutrons and scattered protons in the target-chamber walls and beam tubes, which were made of aluminum. The contribution of the 0.843 MeV line was estimated from the measured line integrals of the 1.014 and 2.211 MeV lines of ^{27}Al and calculations with the nuclear reaction code TALYS [33]. An estimated 50% error was attached to the subtraction of the 0.843 MeV line contribution mainly due to uncertainties arising from the energy spectrum of the particles interacting with the chamber walls.

Some of these lines are also emitted in the β^+ decay of ^{56}Co, strongly produced by the ^{56}Fe$(p,n)^{56}$Co reaction in the measured energy range [22]. Calculations based on the time history of the Fe target irradiation showed, however, that this contribution was completely negligible for all lines considered here. Our data are presented in Fig. 8 together with the Washington data [22] for the 0.847, 1.238, and 1.811 MeV lines. The latter were multiplied by 0.92 to account for the fact that Dyer *et al.* [22] used isotopically enriched ^{56}Fe targets.

We determined furthermore cross sections for deexcitation lines of other Fe isotopes and of ^{56}Co and ^{52}Cr. Below 15 MeV, the strongest contribution comes from lines of ^{56}Co, mainly produced by the ^{56}Fe$(p,n\gamma)^{56}$Co reaction. Above that energy, the one-nucleon separation channels of ^{56}Fe are open, and deexcitation lines of ^{55}Fe are relatively strong reaching the 200 mb range for the 0.931 and 1.316 MeV lines. Those and in particular the 0.931 MeV line are also produced by β^+ decay of ^{55}Co. This contribution was estimated from runs with proton energies below the one-proton separation threshold and activity measurements after irradiation. It did not exceed 3 mb.

Cross sections were obtained for only one line of ^{55}Mn at 0.126 MeV from the ground-state transition of the excited state with a cross section $\approx$10 weaker than the strongest ^{55}Fe lines. Besides that, there were only still weaker ^{55}Mn lines in the spectra from transitions of higher lying levels.

Spallation of one α particle of ^{56}Fe is probably the main source of the 1.434 MeV ^{52}Cr line. This reaction channel is in any case relatively weak in comparison with the equivalent spallation reactions of ^{16}O and ^{24}Mg to the first excited states of ^{12}C and ^{20}Ne, respectively. This may be explained by the higher Coulomb barrier which the α particle faces in ^{56}Fe compared to the two lighter nuclei and probably also stronger α-particle components in the ground- and excited-state configurations of ^{16}O and ^{24}Mg.

4. Lines from α + Fe

The γ-ray spectra from this reaction are completely dominated by ^{56}Fe, ^{58,59}Co, and ^{58,59}Ni lines. As in the case of proton induced reactions, the ^{56}Fe lines are predominantly produced by inelastic scattering off ^{56}Fe. The strongest line at 0.847 keV for the deexcitation of the first excited state of ^{56}Fe has about a factor of 2 smaller cross sections than for proton inelastic scattering, while the 1.238 MeV line from the transition of the second excited state to the first excited state has similar cross sections for both projectiles. Three other lines of ^{56}Fe could be analyzed. Cross-section excitation functions are shown in Fig. 9.

There is excellent agreement with the Washington data [24] for the 1.238 MeV line, while their cross sections of the 0.847 MeV line are larger by about 20% in the range E_α = 15–25 MeV. This can be explained by the fact that the region around the 0.847 MeV line is very complex, with several lines

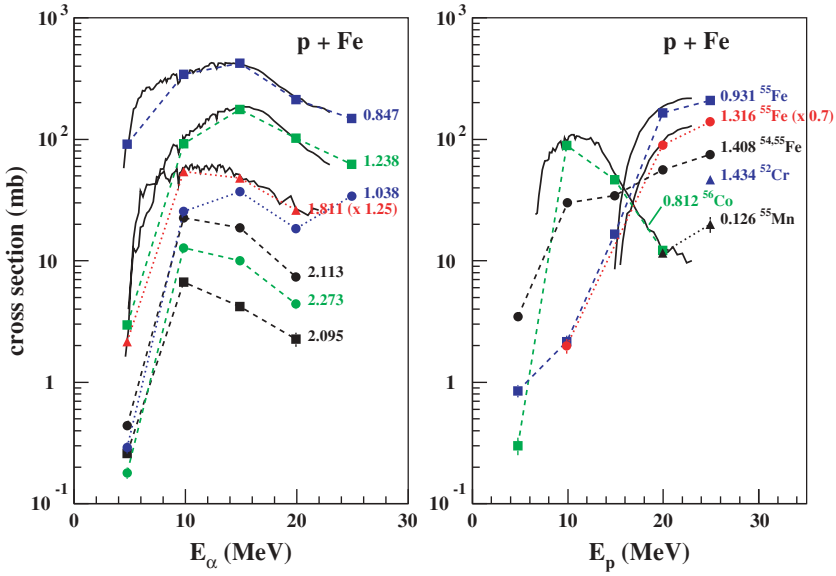

FIG. 8. (Color online) Cross-section excitation functions for ^{56}Fe γ-ray lines (left) and for lines emitted by other Fe isotopes, ^{56}Co, and ^{52}Cr produced by proton interactions with ^{NAT}Fe (right). Continuous lines represent Washington data scaled by a factor of 0.92 to account for the fact that they have been obtained with a isotopically enriched target ^{56}Fe.

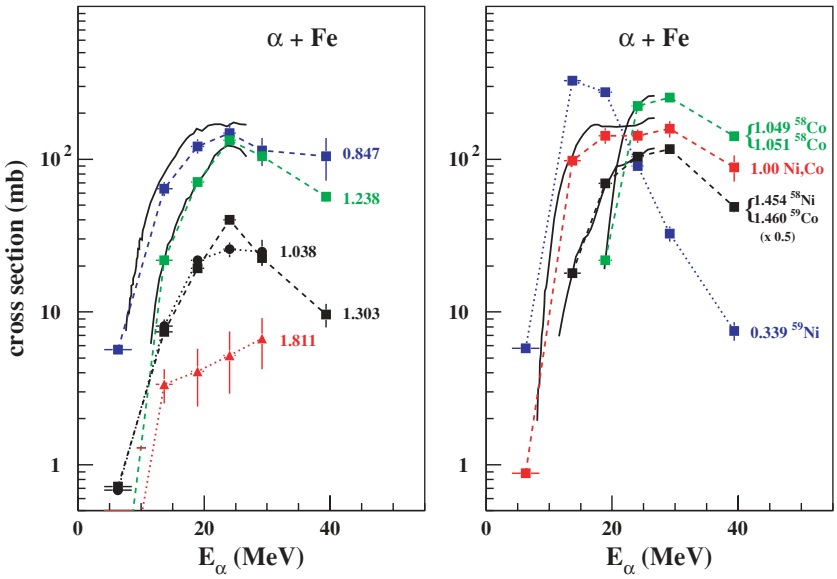

FIG. 9. (Color online) Cross-section excitation functions for ^{56}Fe γ-ray lines (left) and for lines emitted by ^{55}Fe, ^{58,59}Co, and ^{58,59}Ni (right) produced by α-particle interactions with ^{NAT}Fe. Continuous lines show the Washington data.

superimposing partially or completely the ^{56}Fe line. Seamster *et al.* [24] integrated the whole feature including a line of ^{59}Ni at 0.836 MeV and a line at ≈0.855 MeV, with several candidate transitions from Mn, Co, or Ni isotopes, while we extracted the integral of the ^{56}Fe line only. This was done by fits of the whole region including up to four different lines. The line complex was furthermore seated on the triangular feature from neutron inelastic scattering ^{72}Ge$(n, n'\gamma_{0.834})^{72}$Ge making line integration very difficult at higher α-particle energies. Contributions of the 0.843 MeV ^{27}Al line from secondary neutron reactions was subtracted as in the case of proton irradiations. Taken all uncertainties together leads to the relatively large error bars for cross sections of the 0.847 MeV line.

It is remarkable that the cross section for the 0.847 MeV line at 25 and 30 MeV is only slightly larger than that of the 1.238 MeV line, which is feeding the first excited state of ^{56}Fe via the deexcitation of the second excited state 4^+ 2.085 → 2^+ 0.847. This does not leave much cross section for transitions or cascades feeding the 0.847 MeV state without passing by the second excited state at 2.085 MeV. The only line which we analyzed contributing to such feeding is the 1.811 MeV line from the 2^+ 2.658 → 2^+ 0.847 transition, but with a much smaller cross section as in the case of proton inelastic scattering. The two lines at 1.038 and 1.303 MeV (with contribution of the $1/2^-$ 1.301 → $3/2^-$ g.s. transition in ^{59}Ni) are from deexcitation of the 4^+ 3.123 MeV and 6^+ 3.388 MeV levels to the 2.085 MeV level. They have cross sections significantly larger than the 1.811 MeV line, indicating a preference for the population of higher spin states as in proton-induced reactions.

Cross sections of some strong lines from Ni and Co produced by fusion-evaporation reactions and of ^{55}Fe, mainly produced by spallation of ^{56}Fe, are presented in Fig. 9. Many of these lines have multiple origins, and the presumably most important transitions are indicated on the figure. The largest contribution below $E_\alpha = 20$ MeV is from ^{59}Ni lines. Above that beam energy, lines from ^{58}Co and ^{58}Ni become more important. Comparison with the Washington data shows excellent agreement for the sum of 1.049 and 1.051 MeV lines of ^{58}Co and the 1.454 + 1.460 MeV structure. There is reasonable agreement for the feature around 1.0 MeV composed of lines from ^{58,59}Ni and ^{59}Co. Seamster *et al.* [24] give 520 mb at 16 MeV and 125 mb at 24 MeV for the 0.339 MeV line, in reasonable agreement with the present data. The spectra for this reaction show many more lines with cross sections exceeding several mb, but only a part of them were analyzed given the complexity of some structures of multiple superimposed lines with sometimes non-Gaussian shapes.

V. COMPARISON WITH CALCULATIONS

The interpretation of the γ-ray spectra observed during solar flares requires a good knowledge of the γ-ray production cross sections for proton, ^{3}He, and α-particle induced reactions. When experimental cross-section data are not available, theoretical calculations using nuclear reaction models become essential. Then, it is of primary importance to check the validity of the calculated cross sections by confronting them with existing experimental counterparts.

Different nuclear reaction mechanisms are assumed to occur in the investigated energy range such as the compound nucleus formation and the direct and preequilibrium interaction processes. For the calculations, we decided to take advantage of the development of modern global nuclear reaction codes like TALYS [33] and EMPIRE [34]. Both include the major nuclear reaction mechanisms at energies below ≈250 MeV per nucleon and use comprehensive libraries of nuclear structure data. This enables in particular the calculation of the total γ-ray emission produced by light particle induced interactions in the important energy range for solar flares. In the following, we show the calculations carried out using the EMPIRE-II computer code [34].

We have restricted ourselves to the calculation of proton induced reactions for which a comprehensive study on nuclear

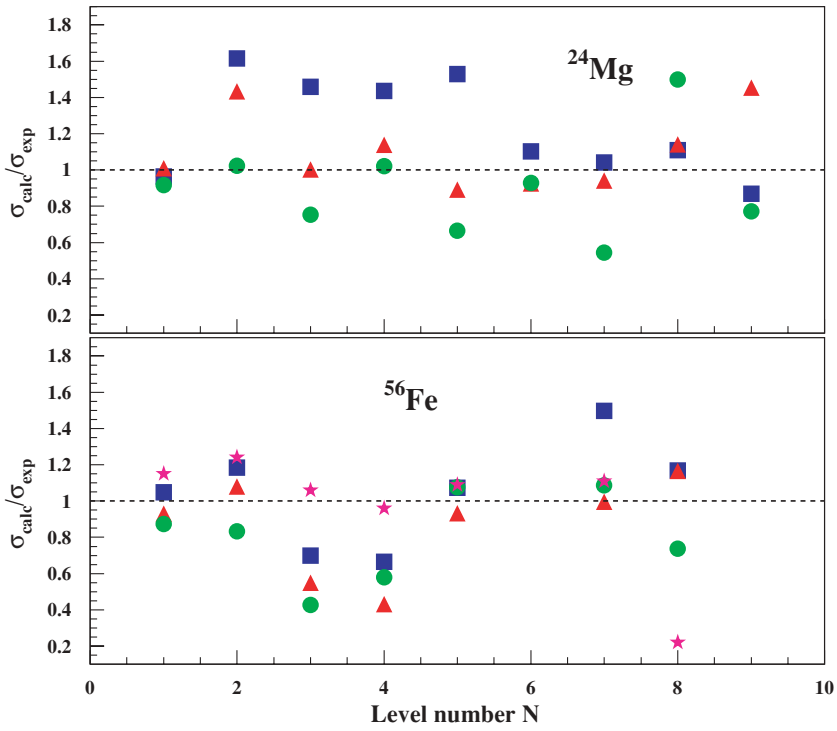

FIG. 10. (Color online) Ratio of calculated to measured cross sections for deexcitation lines induced by inelastic proton scattering off ^{56}Fe at $E_p = 5$ MeV (stars) and off ^{56}Fe and ^{24}Mg at $E_p = 10$ MeV (filled squares), 15 MeV (filled triangles) and 20 MeV (filled circles). The calculations at 5, 10, and 15 MeV are the sum of direct and HF contributions; at 20 MeV, the sum of HMS and direct contributions. The ratios are plotted as a function of the number N of the deexciting level, ordered by increasing excitation energy, starting with $N = 0$ for the ground state.

reaction optical potentials has been carried out [35]. The calculation of α-particle induced reaction cross sections is not reported in the present paper because it requires an extensive research of the optical potential parameters indispensable to the analysis. In fact, satisfactory optical potentials for α particles are available only for few nuclei, and one has to consistently fit elastic and inelastic α-particle scattering cross sections to extract these parameters.

We present first the results for the lines of ^{24}Mg and ^{56}Fe, where the different reaction mechanisms contribute in a similar way, while the calculations for the 4.438 MeV line are treated separately. They are particular because of the much lower level densities of nuclei in the CNO mass region compared to Mg and Fe. In particular, the 4.438 MeV line originates from the deexcitation of the only particle-bound excited state of ^{12}C, while ^{24}Mg has several tens and ^{56}Fe more than 100 levels below their respective particle emission thresholds. One important effect is a drastic reduction of the population of the 4.439 MeV level by cascades from higher lying states of ^{12}C, reducing thereby the importance of, e.g., preequilibrium reactions with respect to the direct reaction mechanism in the inelastic scattering reactions.

A. Lines from ^{24}Mg and ^{56}Fe

For both nuclei, we measured cross sections of several lines produced by inelastic scattering, and for some of them in an energy range covering 15 or even 20 MeV for lines from the lowest lying excited states. This permitted us to study the transition from the region of dominating compound nucleus reactions at low energies to the region of prominent preequilibrium and direct reactions. The direct reaction mechanism is only important for low-lying collective levels such as the first two excited states of the ground-state rotational band in ^{24}Mg. However, even for these states its contribution does not exceed 20% of the cross section below $E_p = 25$ MeV.

The contribution of a compound nucleus mechanism was calculated using an advanced implementation of the statistical Hauser-Feshbach (HF) theory (HF cross section, depicted by dashed curves in Figs. 11–16) of EMPIRE-II. It shows good agreement with the measured cross sections of the inelastic scattering lines below 15 MeV proton energy for both nuclei. Figure 10 shows the ratio of calculated to measured cross sections for these lines at $E_p = 5$ MeV for ^{56}Fe and at 10 and 15 MeV for both nuclei. The mean deviation from unity is less than 20%, except for the ratios of ^{24}Mg lines at 10 MeV, where it is slightly less than 30%.

Above 15 MeV, the HF calculations underestimate the inelastic scattering cross sections typically by a factor of 2 at $E_p = 20$ MeV and by a factor of 3 at $E_p = 25$ MeV. Among the different approaches to the preequilibrium reactions proposed by EMPIRE-II, only the hybrid Monte Carlo simulation (HMS), a method inspired by the intranuclear cascade approach, gave cross sections comparable to the experimental ones. The other approaches underestimated considerably the experimentally measured cross sections, even by adding HF and direct contributions. In fact, the HMS cross sections, with the direct contributions added, showed a similar good agreement with the measured cross sections for the inelastic lines above 15 MeV (see Fig. 10) as the HF calculations up to 15 MeV.

This is furthermore illustrated in Fig. 11, where we represent the direct, HF, and HMS calculations for the line at 1.369 MeV. The best reproduction of the experimental cross-section excitation functions for the inelastic lines of

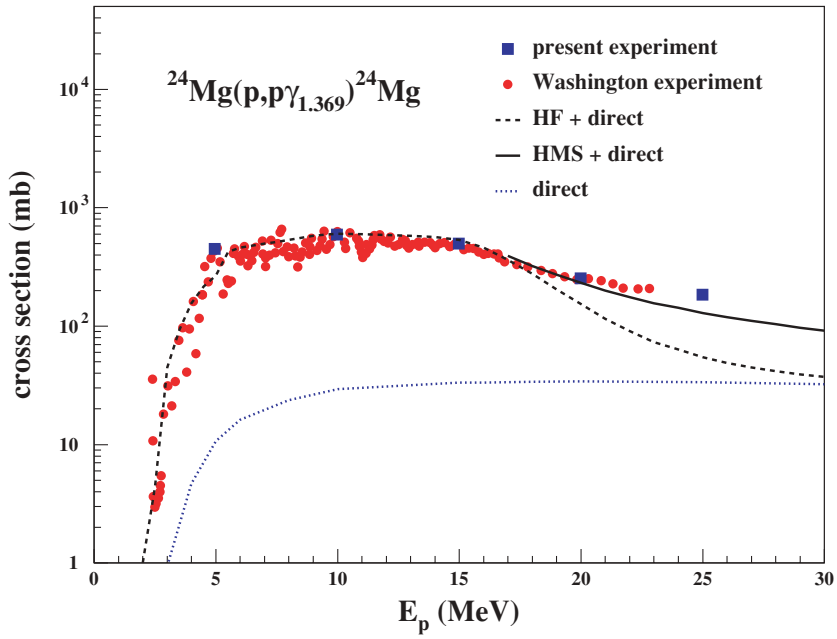

FIG. 11. (Color online) Excitation function for the 1.369 MeV γ-ray line produced in proton inelastic scattering off ^{24}Mg. The dashed line is the sum of Hauser Feshbach and direct reaction calculations. The solid line above 17 MeV shows the sum of preequilibrium HMS and direct reaction calculation. Error bars as in Fig. 16.

^{24}Mg was finally obtained by taking HF cross sections up to 17 MeV and above that energy the HMS cross sections, adding to both the direct contribution. We tested this recipe on other lines produced in proton reactions with ^{24}Mg. The overall agreement with measured data for the spallation lines was found to be as good as for the inelastic lines. Figure 12 shows cross sections for the strongest spallation line of ^{24}Mg composed of the 1.636 and 1.634 MeV lines originating from the deexcitation of the second and first excited states of the ^{23}Na and ^{20}Ne nuclei, respectively.

For the inelastic lines from proton scattering off ^{56}Fe, the HMS cross sections showed in many cases already at 10 MeV an equally good description of measured data as that obtained by the HF calculations and a better one at 15 MeV. This is illustrated in Fig. 13 for the 2.113 MeV line of ^{56}Fe, which shows a typical cross-section excitation function. Similar agreement was found for all lines from inelastic scattering obtained in the present experiment. However, for the lines from the first two excited states of ^{56}Fe at 0.847 and 1.238 MeV, the calculations seemed to show a progressive underestimation of the data at E_p above $\approx$ 15 MeV. This was especially obvious when comparing with all experimentally available cross sections including the data of Lesko *et al.* [25] who measured cross sections for these two lines up to E_p = 50 MeV.

Comparison of calculations with a compilation of experimental data is shown in Fig. 14 for the 0.847 MeV line. As mentioned above, the HF calculations satisfactorily reproduce

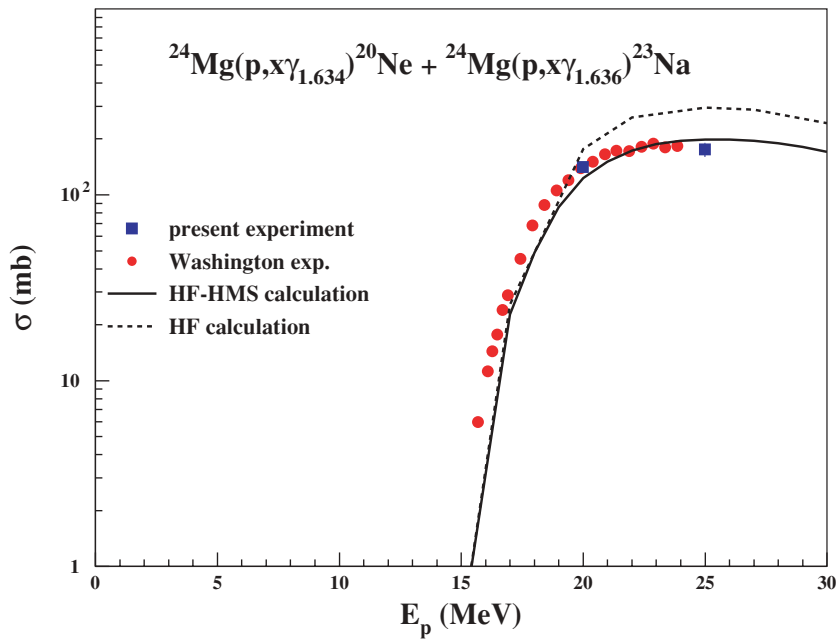

FIG. 12. (Color online) Excitation function for the sum of the spallation lines of ^{20}Ne at 1.634 MeV and of ^{23}Na at 1.636 MeV. Solid lines represent the HF calculations matched to the HMS ones at E_p = 17 MeV. Error bars as in Fig. 16.

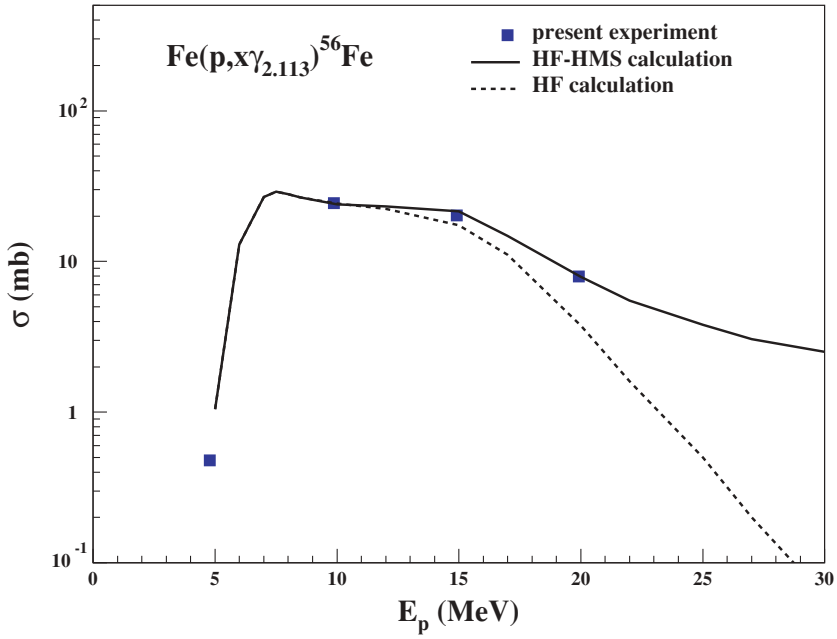

FIG. 13. (Color online) Excitation functions for the 2.113 MeV γ-ray line produced in proton inelastic scattering off ^{56}Fe. Error bars as in Fig. 16.

the measured data up to $E_p \approx 15$ MeV. Above this energy value, the HMS calculations are more adequate, but they do not satisfactorily reproduce the higher energy data and particularly the data of Lesko *et al.* [25] above $E_p = 30$ MeV. Even if one considers the contributions of γ-ray lines of energies close to 0.847 MeV (e.g., the line at 0.841 MeV in ^{55}Fe) and sums them to that of the main line, one still cannot account for the high-energy data. The same holds for the 1.238 MeV line of ^{56}Fe. At the moment, it is not clear if that is a general behavior of inelastic scattering to low-lying collective levels. There is a similar indication for lines from low-lying collective levels in ^{24}Mg where the calculations also tend to slightly underestimate measured data at $E_p \geqslant 20$ MeV (see Fig. 11).

In this respect, lines from proton induced spallation reactions of ^{56}Fe are much better reproduced than the inelastic lines from the first two excited states of ^{56}Fe. An example is shown in Fig. 15 for the lines at 1.4081 and 1.4084 MeV resulting from deexcitations in ^{54}Fe and ^{55}Fe, respectively, which are not resolved experimentally. The measured data for these lines are quite well reproduced by the calculated cross sections up to $E_p = 40$ MeV. The cross sections measured at $E_p < 15$ MeV are not due to a spallation reaction but originate from the ^{54}Fe$(p, p'\gamma_{1.4082})^{54}$Fe proton scattering off the ^{54}Fe isotope present in the iron target foil of natural isotopic composition (the abundance of ^{54}Fe being of 5.8%).

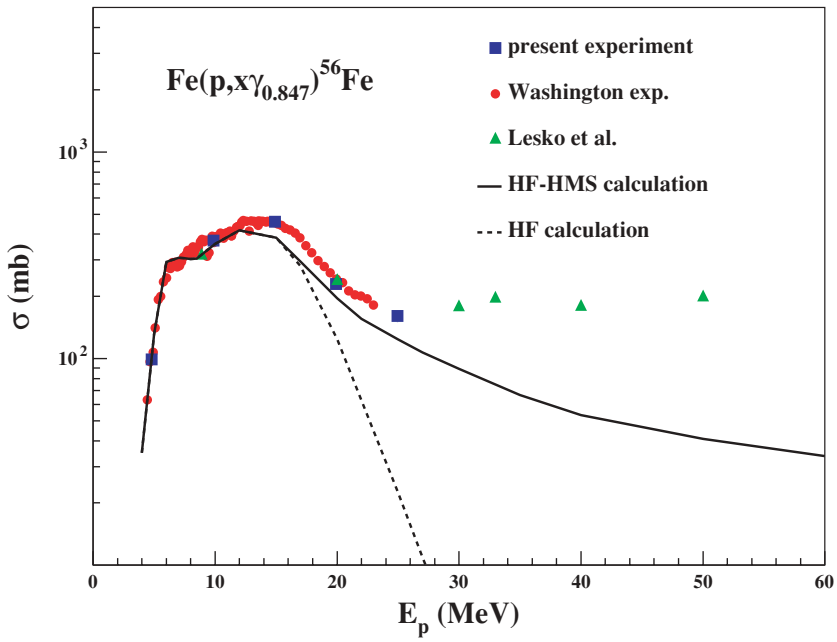

FIG. 14. (Color online) Excitation functions for the 0.847 MeV γ-ray line produced mainly in proton inelastic scattering off ^{56}Fe. The calculation for the 847 keV γ ray includes the contribution of the 841 keV line from ^{55}Fe. Error bars as in Fig. 16.

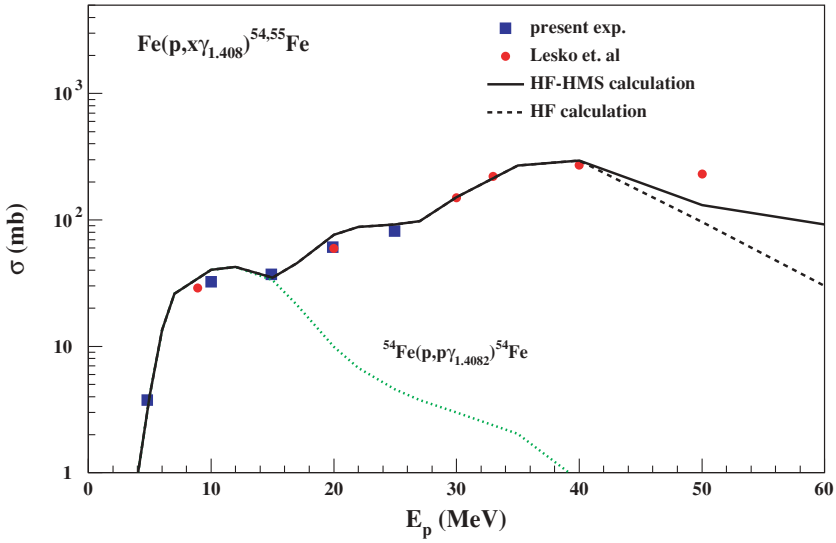

FIG. 15. (Color online) Excitation functions for the 1.408 MeV γ-ray line produced in proton inelastic scattering off ^{54}Fe and in spallation reactions mainly of ^{56}Fe to ^{54}Fe$^{\star}_{1.408}$ and ^{55}Fe$^{\star}_{1.408}$. The inelastic scattering off ^{54}Fe is shown separately by the dotted line. Error bars as in Fig. 16.

B. The 4.438 MeV γ-ray line from ^{12}C

The calculated cross sections for the γ-ray line at 4.438 MeV produced by inelastic proton scattering off ^{12}C are compared with the present and the Washington data in Fig. 16. The measured data are particularly well reproduced by the sum of the calculated HF and direct cross sections, the latter being evaluated using the coupled-channels method applied to the states of the first rotational band in ^{12}C. The optical potential of A. S. Meigooni *et al.* [36] has been used to evaluate the contributions of the different nuclear reaction mechanisms to the total reaction cross section. The preequilibrium contribution for this reaction was found to be negligible.

Since the 4.438 MeV line is also produced in spallation reactions of protons with ^{16}O, we have calculated the corresponding reaction cross sections. While the calculated cross sections using the HMS approach are in good agreement with the experimental data (see Fig. 17) those calculated following the HF theory are far below the experiment and are not reported here. Notice that in this calculation, we applied the level density approach which uses the Fermi gas deformation dependent collective effects with the level density parameters a being derived from the shell model.

C. Summary of nuclear reaction calculations

The present preliminary calculations are promising and have shown some general trends which distinguish the different nuclear reaction models. At energies below about 15 MeV where the compound nucleus mechanism dominates, Hauser-Feshbach calculations describe very satisfactorily the data. Above that energy, the preequilibrium mechanism becomes important, and the hybrid Monte Carlo simulation calculations

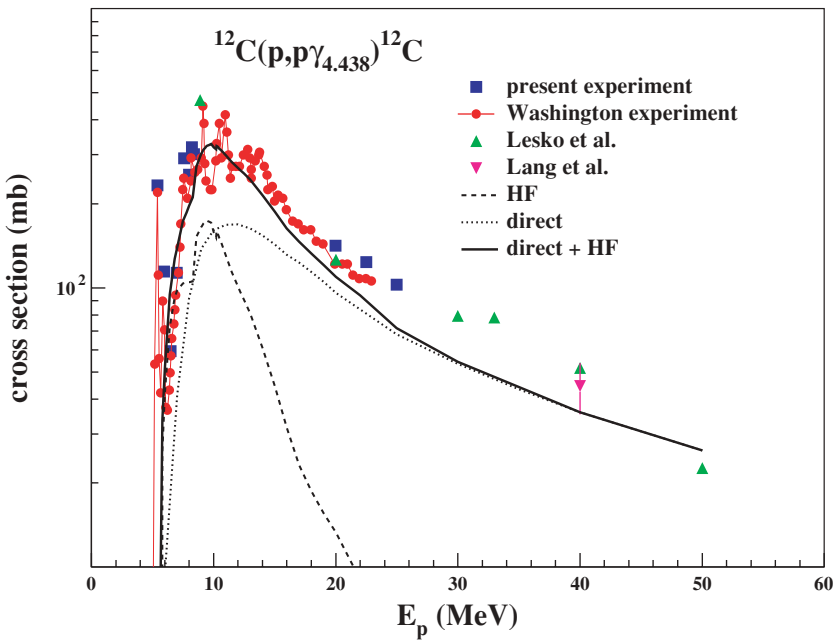

FIG. 16. (Color online) Excitation functions for the 4.438 MeV γ-ray line produced in proton inelastic scattering off ^{12}C. The solid line represents the sum of Hauser-Feshbach (HF) and direct reaction calculations. With the exception of the Lang *et al.* data, the uncertainties on the absolute normalization of the measured excitation functions are not shown in this and the preceding and following figures. They are typically 15% for the Washington experiment and 15–17% for Lesko *et al.* Please see text for the present experiment.

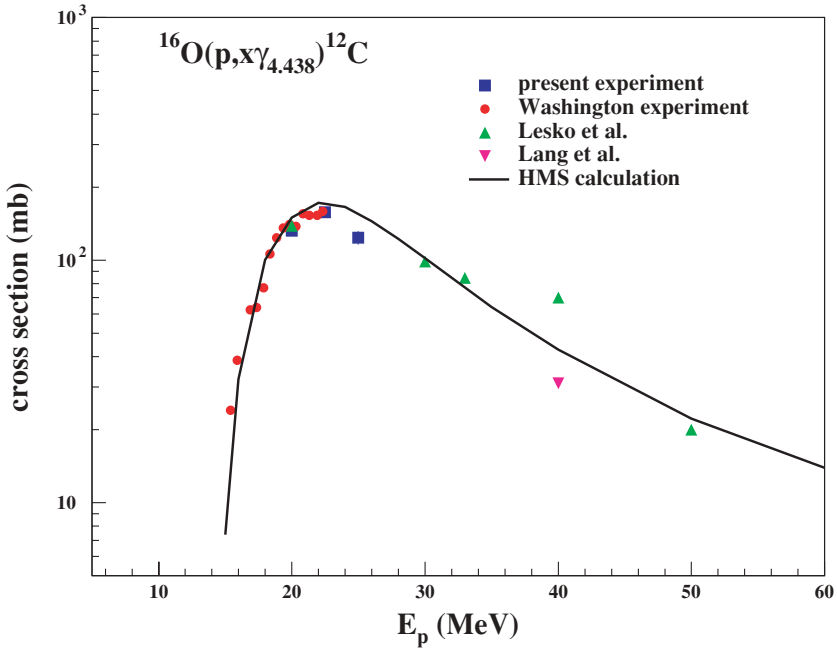

FIG. 17. (Color online) Excitation functions for the 4.438 MeV γ-ray line produced in the spallation of ^{16}O. The solid line represents the preequilibrium hybrid Monte Carlo (HMS) calculation with the nuclear reaction code EMPIRE-II. Error bars as in Fig. 16.

are usually much closer to the data than other preequilibrium calculations proposed in the EMPIRE-II code. HF and HMS calculations match in general around 15 MeV, and together they describe the data very satisfactorily up to at least 25 MeV.

There may be a problem in the calculations above 20 MeV for inelastic scattering to the low-lying collective levels which are also strongly excited by the direct reaction mechanism. This is obvious for inelastic scattering to the first two levels of ^{56}Fe and—to a minor extent—for the first three to four levels of ^{24}Mg, while ^{12}C is a special case as discussed above. Improvements for these cases may be possible by a careful study of coupling schemes and optical potential parameters in direct reaction calculations. Preliminary calculations with an extended coupling scheme for the ^{56}Fe ground-state band point to that direction. The calculations must eventually also be extended to α-particle induced reactions but require beforehand extensive work on optical potentials. These developments are, however, beyond the scope of this paper and will be presented later.

VI. CONCLUDING REMARKS

We measured cross-section data for about 50 different γ-ray lines produced in proton and α-particle interactions with ^{12}C, ^{16}O, ^{24}Mg, and Fe with cross sections exceeding several mb. For many of these lines, no γ-ray production cross sections existed before in the literature. Where a comparison with existing data was possible, good to excellent agreement could be observed, especially with the data of the Washington experiments [22–24] and often also with Lesko *et al.* [25].

These data were obtained in the interesting energy range for solar flares, and many of the measured cross-section excitation functions may be used directly for the analysis and interpretation of the γ-ray emission of solar flares. An example are the ^{59}Ni lines which are predominantly produced by α-particle reactions with ^{56}Fe. This can be used to determine the α/p ratio as it was done by Mandzhavidze *et al.* [37] in 20 flares from the observed fluence ratio of the 0.339 MeV line of ^{59}Ni and the 0.847 MeV line of ^{56}Fe. Strongly produced spallation lines of ^{24}Mg and ^{56}Fe, such as the 0.440 and 0.931 MeV lines of ^{23}Na and ^{55}Fe, respectively, can be used to deduce the spectral index of the energy distribution of the accelerated particles because their reaction thresholds are higher than those from inelastic scattering off ^{24}Mg and ^{56}Fe.

Preliminary calculations with modern global nuclear reaction codes such as EMPIRE-II [34] or TALYS [33] are encouraging and show the potential of the data to test the different nuclear reaction models. Those calculations can be used to predict the total nuclear γ-ray production in solar flares. An example for a comparison of predictions utilizing results from those codes with the observed γ-ray emission of a strong solar flare is presented in Ref. [38].

Furthermore, we extracted high-precision line profiles for the 4.438 MeV γ-ray line of ^{12}C for α-particle inelastic scattering off ^{12}C and spallation of ^{16}O from reaction threshold energy to 37.5 MeV and for some proton energies not covered in a previous experiment [12]. The complete set of line shapes will be used to deduce the parameters necessary for the calculation of the 4.438 MeV line shape in solar flares.

ACKNOWLEDGMENTS

We thank the staff of the IPN Orsay tandem accelerator for their advice and efficient help in the setup phase and during the experiment.

APPENDIX

In addition to the cross sections shown in the figures of the present paper, we also supply numerical values for all extracted cross sections and the Legendre polynomial parameters of the γ-ray angular distributions in the EPAPS document [39].

[1] R. Ramaty, B. Kozlovsky, and R. E. Lingenfelter, Astrophys. J. Suppl. Ser. **40**, 487 (1979).
[2] R. J. Murphy, B. Kozlovsky, and R. Ramaty, Astrophys. J. **331**, 1029 (1988).
[3] W. T. Vestrand, G. H. Share, R. J. Murphy, D. J. Forest, E. Rieger, E. L. Chupp, and G. Kanbach, Astrophys. J. Suppl. Ser. **120**, 409 (1999).
[4] R. J. Murphy, R. Ramaty, B. Kozlovsky, and D. V. Reames, Astrophys. J. **371**, 793 (1991).
[5] R. Ramaty, N. Mandzhavidze, B. Kozlovsly, and R. J. Murphy, Astrophys. J. **455**, L193 (1995).
[6] G. H. Share and R. J. Murphy, Astrophys. J. **485**, 409 (1997).
[7] G. H. Share, R. J. Murphy, J. Kiener, and N. de Séréville, Astrophys. J. **573**, 464 (2002).
[8] R. P. Lin *et al*., Astrophys. J. Lett. **595**, 69 (2003).
[9] C. Winkler *et al*., Astron. Astrophys. **411**, L1 (2003).
[10] J. Kiener, M. Gros, V. Tatischeff, and G. Weidenspointner, Astron. Astrophys. **445**, 725 (2006).
[11] J. J. Kolata, R. Auble, and A. Galonsky, Phys. Rev. **162**, 957 (1967).
[12] J. Kiener, M. Berheide, N. L. Achouri, A. Boughrara, A. Coc, A. Lefebvre, F. de Oliveira Santos, and Ch. Vieu, Phys. Rev. C **58**, 2174 (1998).
[13] J. Kiener, N. de Séréville, and V. Tatischeff, Phys. Rev. C **64**, 025803 (2001).
[14] G. H. Share and R. J. Murphy, in *GAMMA 2001: Gamma-Ray Astrophysics 2001*, edited by S. Ritz, N. Gehrels, and C. Shrader, AIP Conf. Proc. No. 587 (AIP, New York, 2001), p. 603.
[15] P. J. Nolan, F. A. Beck, and D. B. Fossan, Annu. Rev. Nucl. Part. Sci. **44**, 561 (1994).
[16] D. C. Radford, Nucl. Instrum. Methods A **361**, 297 (1995).
[17] CERN Program Library Office (Online), http://wwwasdoc.web.cern.ch/wwwasdoc/geant_html3/geantall.html
[18] A. J. Ferguson, *Angular Correlation Methods in Gamma-Ray Spectroscopy* (North-Holland, Amsterdam, 1965).
[19] M. O. Thompson, GENPLOT and RUMP documentation, 1996, http://www.genplot.com/doc/index.htm
[20] M. Mayer, in *Proceedings of the 15th International Conference on the Application of Accelerators in Research and Industry*, AIP Conf. Proc. No. 475, edited by J. L. Duggan and I. L. Morgan (AIP, New York, 1999), p. 541. See also http://www.rzg.mpg.de/mam/
[21] J. F. Ziegler, *The Stopping and Range of Ions in Matter* (Pergamon, New York, 1985). See also http://www.srim.org/index.htm#SRIM
[22] P. Dyer, D. Bodansky, A. G. Seamster, E. B. Norman, and D. R. Maxson, Phys. Rev. C **23**, 1865 (1981); additional γ-ray angular distributions not shown in the article have been provided by R. Ramaty (private communication).
[23] P. Dyer, D. Bodansky, D. D. Leach, E. B. Norman, and A. G. Seamster, Phys. Rev. C **32**, 1873 (1985).
[24] A. G. Seamster, E. B. Norman, D. D. Leach, P. Dyer, and D. Bodansky, Phys. Rev. C **29**, 394 (1984).
[25] K. T. Lesko, E. B. Norman, R. M. Larimer, S. Kuhn, D. M. Meekhof, S. G. Crane, and H. G. Bussell, Phys. Rev. C **37**, 1808 (1988).
[26] F. L. Lang, C. W. Werntz, C. J. Crannell, J. I. Trombka, and C. C. Chang, Phys. Rev. C **35**, 1214 (1987).
[27] J. Narayanaswamy, P. Dyer, S. R. Faber, and S. M. Austin, Phys. Rev. C **24**, 2727 (1981).
[28] R. B. Firestone, V. S. Shirley, C. M. Baglin, S. Y. Frank Chu, J. Zipkin, *Table of Isotopes* (Wiley, New York, 1996).
[29] W. Zobel, F. C. Maienschein, J. H. Todd, and G. T. Chapman, Nucl. Sci. Eng. **32**, 392 (1968).
[30] P. Leleux (private communication).
[31] G. M. Crawley and G. T. Garvey, Phys. Rev. **160**, 981 (1967); data were taken from the EXFOR library at http://www.nndc.bnl.gov/exfor3/exfor00.htm
[32] D. K. Hasell, N. E. Davison, T. N. Nasr, B. T. Murdoch, A. M. Sourkes, and W. T. H. van Oers, Phys. Rev. C **27**, 482 (1983); data were taken from the EXFOR library at http://www.nndc.bnl.gov/exfor3/exfor00.htm
[33] A. J. Koning, S. Hilaire, and M. C. Duijvestijn, in *International Conference on Nuclear Data for Science and Technology–ND2004*, AIP Conf. Proc. No. 769 (AIP, Melville, 2005), p. 1154.
[34] M. Herman, P. Oblozinský, R. Capote, M. Sin, A. Trkov, A. Ventura, and V. Zerkin, in *International Conference on Nuclear Data for Science and Technology–ND2004*, AIP Conf. Proc. No. 769 (AIP, Melville, 2005), p. 1184; also available at http://www.nndc.bnl.gov/empire-2.18
[35] A. J. Koning and J. P. Delaroche, Nucl. Phys. **A713**, 231 (2003).
[36] A. S. Meigooni, R. W. Finlay, J. S. Petler, and J. P. Delaroche, Nucl. Phys. **A445**, 304 (1985).
[37] N. Mandzhavidze, R. Ramaty, and B. Kozlovsky, Astrophys. J. **518**, 918 (1999).
[38] J. Kiener, V. Tatischeff, G. Weidenspointner, M. Gros, and A. Belhout, in *Tours Symposium on Nuclear Physics VI*, AIP Conf. Proc. No. 891, edited by M. Arnould, M. Lewitowicz, H. Emling, H. Akimune, M. Ohta, H. Utsunomiya, T. Wada, and T. Yamagata (AIP, Melville, 2007), p. 254.
[39] See EPAPS Document No. E-PRVCAN-76-001710 for numerical values of cross sections and Legendre polynomial parameters. For more information on EPAPS, see http://www.aip.org/pubservs/epaps.html.